

Restoration of multiphase salt tectonic deformation using passive strain markers

Chris Kirkham | Joe Cartwright

Department of Earth Sciences, University of Oxford, Oxford, UK

Correspondence

Chris Kirkham, Department of Earth Sciences, University of Oxford, South Parks Road, Oxford, OX1 3AN, UK.
Email: christopher.kirkham@earth.ox.ac.uk

Abstract

Several salt basins globally have been subject to multiphase deformation. The geometry of structures formed within a salt sheet during an early phase of deformation can be concealed by overprinting during later deformation phases, impeding an informed investigation into the early drivers for salt flow. The layered Messinian Evaporites in the deep basins of the Eastern Mediterranean have undergone a Late Messinian phase of deformation, punctuated by truncation of the top of the deformation structures, followed by a Late Pliocene-Recent phase of deformation. Seismic reflection data show that the Messinian Evaporites are internally dominated by contraction structures that verge basinward in the Late Pliocene-Recent flow direction, with several apparent detachments. Planform linear trails of fluid escape pipes, documented in the North Levant Basin, that cross-cut the Messinian Evaporites present natural passive markers for the internal flow kinematics of the salt sheet throughout the Late Pliocene-Recent phase of deformation. Using the Couette (simple shear) strain profile implied by the fluid escape pipes, we remove the effects of the Late Pliocene-Recent deformation through cross section and map restorations. The subsequent geometries are far simpler, with upright folds that are now vertically aligned. Once apparently detached structures are demonstrably connected through the Messinian Evaporites. The vergence of the present day intrasalt folds can be taken as an indicator for the Late Pliocene-Recent flow direction and distinct deformation geometries that connect at various levels through the salt sequence once retro-deformed can assist when interpreting the salt flow profile. The retro-deformation is essential for how intra-Messinian deformation and its drivers are interpreted going forward. Furthermore, simple shear deformation results in erroneous apparent percentage shortening calculations as line length is not conserved, obscuring the strain from the pre-Pliocene deformational phase. The methodology employed here has important implications for all salt basins that have undergone multiphase deformation.

KEYWORDS

Eastern Mediterranean, fluid escape pipes, Messinian Evaporites, multiphase deformation, retro-deformation, salt tectonics, sedimentary basin, structural restoration

This is an open access article under the terms of the Creative Commons Attribution License, which permits use, distribution and reproduction in any medium, provided the original work is properly cited.

© 2021 The Authors. *Basin Research* published by International Association of Sedimentologists and European Association of Geoscientists and Engineers and John Wiley & Sons Ltd

1 | INTRODUCTION

One of the major unresolved questions in salt tectonics is how an originally thick, basin scale salt sheet flows and deforms internally in response to different drivers for the deformation, be it differential loading, differential uplift/subsidence and tilting, or regional plate kinematics (Albertz & Ings, 2012; Brun & Fort, 2011; Gemmer et al., 2004; Rowan et al., 2004). Seismic investigations of this relationship have dominated the research into this problem for the last 50 years but have focused largely on analysing the response of the overburden to the boundary conditions driving the deformation and inferring the flow of the salt indirectly from these observations (reviewed by Jackson et al., 2015). In the past decade, as seismic imaging capabilities of salt tectonic provinces have improved, it has become possible to see the internal structure of the deformed salt, as opposed to the observations of the deformed geometry being solely restricted to the upper and lower boundaries of the salt bodies. Using 3D seismic data, salt sequences in the Southern Permian Basin of the North Sea (Van Gent et al., 2011), the Santos Basin (Fiduk & Rowan, 2012) offshore Brazil and the Levant Basin of the Eastern Mediterranean (Cartwright et al., 2012) were all found to exhibit internal deformational patterns that markedly contrasted with the deformed geometry of the overburden, prompting questions regarding the origin and significance of the contrasting deformational styles within and above the salt.

The approach adopted by these studies has a potentially far wider applicability to tackle more fundamental questions of salt kinematics. By marrying overburden deformational response to internal flow kinematics of the salt it should be possible to link quantitative observations of intrasalt reflection geometry and gross thickness variation of the deformed salt body to the generally much better constrained structure of the overburden. This approach was demonstrated by Cartwright et al. (2012) by measuring contractional strain at different levels within a highly deformed succession of Messinian Evaporites in the Levant Basin, and relating the vertical strain profile to the flow behaviour of the salt. However, this analysis was predicated on there being a single phase of deformation that linked the overburden deformation to those strain measurements inside the salt sheet. At the upper end of the spectrum, multiphase deformation has previously been proposed to explain the internal deformation within the Messinian Evaporites (Kartveit et al., 2018; Netzeband et al., 2006). This deformation has been interpreted to have taken place during one or more syn-Messinian episodes of deformation (Bertoni & Cartwright, 2007; Gvirtzman et al., 2013; Netzeband et al., 2006) and one or more Late Pliocene to Recent deformational episodes (Ben Zeev & Gvirtzman, 2020; Cartwright & Jackson, 2008) that were likely applied over most of the Levant Basin, separated

Highlights

- Fluid escape pipes calibrate the Pliocene-Recent Couette flow profile through the Messinian Evaporites.
- Restoration to remove the recent simple shear reveals the Late Messinian geometry of intrasalt folds.
- Retro-deformation has important implications for interpreting pre-Pliocene deformation and drivers.
- Structures that reconnect once retro-deformed imply that intrasalt structures can be used as kinematic markers.
- Line length is not conserved during simple shear. Simple shear obscures the original strain.

by an Early-Mid Pliocene period of quiescence (Elfassi et al., 2019). For simplicity and the purposes of this paper, we divide these episodes into main two phases of deformational history (pre-Pliocene—Phase 1; Late Pliocene to Recent—Phase 2). Marginal uplift and basin tilting are proposed as the salt flow driver during Phase 1 (Bertoni & Cartwright, 2007; Gvirtzman et al., 2013; Netzeband et al., 2006), as well as for Phase 2 but with an additional contribution from differential loading (Ben Zeev & Gvirtzman, 2020; Elfassi et al., 2019; Kirkham et al., 2019; Zucker et al., 2020). This then automatically raises the question of how to relate the overburden deformation to the internal deformation in the salt, and how the strain distribution in the salt from these two phases may be distinguished.

The recent recognition of fluid escape pipe trails in the North Levant Basin of the Eastern Mediterranean by Cartwright et al. (2018), Kirkham et al. (2019) and Oppo et al. (2020) may prove to be a potential means of resolving this problem. The salt tectonics focused studies of Cartwright et al. (2018) and Kirkham et al. (2019) identified a series of five planform linear trails of fluid escape pipes that transect the full extent of the thick Messinian Evaporites and root to the crest of two major pre-salt anticlines named Oceanus and Saida-Tyr (Figure 1). A single fluid escape pipe trail is sourced from Oceanus (Figure 1), whereas four fluid escape pipe trails root to Saida-Tyr (Kirkham et al., 2019; Oppo et al., 2020). These trails are oriented NW-SE, are 3–7 km in length and consist of a series of progressively deformed fluid escape pipes connected to pockmarks at their outlets that increase in age to the NW in all the five trails. These pockmarks formed episodically over an approximately two million year interval in the Late Pliocene to Recent. The onset

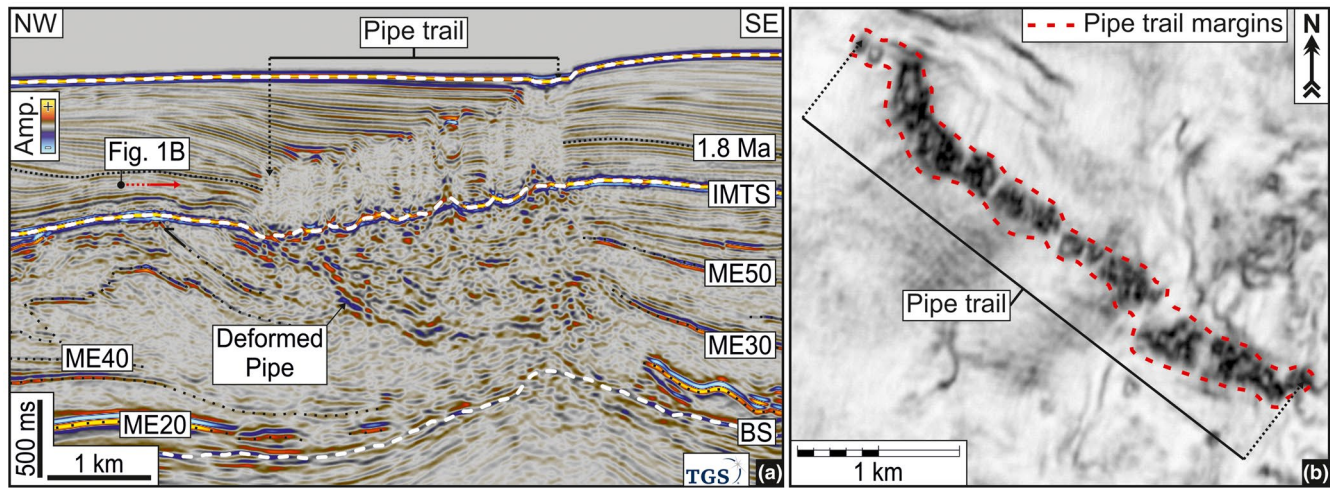


FIGURE 1 Calibrating the kinematic of the salt layer in the North Levant Basin during the Late Pliocene to Recent using fluid escape pipes (modified from Cartwright et al., 2018). (a) A seismic profile through the NW-SE oriented Oceanus fluid escape pipe trail overlying the pre-salt anticline, named Oceanus, offshore Lebanon (see Figure 2a for location). BS, Base Salt; IMTS, intra-Messinian Truncation Surface. (b) A variance slice through the Oceanus fluid escape pipe trail (see Figure 1a for slice position), showing the NW-SE linear distribution of the fluid escape pipes (red dashed line marks the margins of the fluid escape pipe trail). Seismic data courtesy of TGS [Colour figure can be viewed at wileyonlinelibrary.com]

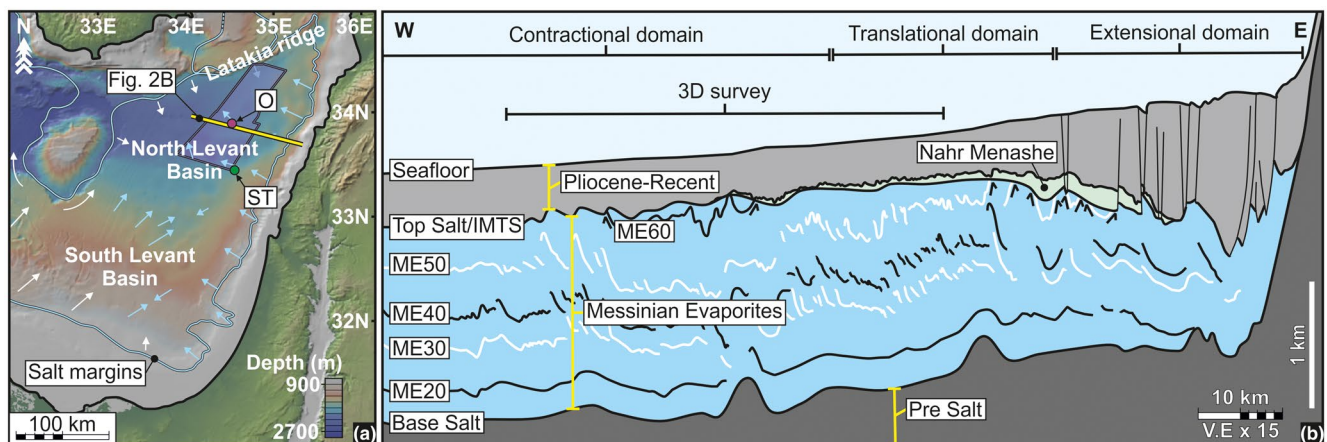


FIGURE 2 Location of the study area and the recent salt flow directions in the Levant Basin. (a) A bathymetric map showing the location of the 3D seismic survey, in the study area of the North Levant Basin. The white arrows represent inferred recent salt flow directions and the light blue arrows represent observed and recorded recent salt flow directions (modified from Allen et al., 2016; Cartwright & Jackson, 2008; Cartwright et al., 2018; Kirkham et al., 2019; Zucker et al., 2020). (b) A regional 2D cross section through the study area (see Figure 2a for location), showing the main marker horizons and evolution from extensional domain marginally, to the basinward translational and contractional domains. IMTS, intra-Messinian Truncation Surface [Colour figure can be viewed at wileyonlinelibrary.com]

of fluid venting from the Oceanus and Saida-Tyr pre-salt anticlines was approximately synchronous at 1.7 Ma (Figure 1) and was contemporaneous to the Phase 2 Late Pliocene to Recent deformation in the North Levant Basin recorded by thin-skinned growth faults at the eastern marginal pinch-out of the Messinian Evaporites (Kirkham et al., 2019). The fluid escape pipe trails are located close to the basin margin (Figure 2a), where the overburden is in a translational domain (Figure 2b) of a classical gravity tectonic system. The fluid escape pipes emanated from reservoirs located in the pre-salt succession were originally vertical through the salt but were deformed into their current configurations by the flow of the

salt. Fluid escape pipes form vertical columnar zones of low coherency in seismic reflection data (Løseth et al., 2011) that are typically poorly imaged and challenging to interpret in salt (Kirkham et al., 2018); however, the deformed fluid escape pipes through the salt in the North Levant Basin are imaged in part due to their oblique geometry. The pockmarks that formed at contemporaneous seafloors were systematically offset NW by translation of the post-salt in the basinward salt flow direction (Figure 1). Based on these observations, Cartwright et al. (2018) argued that these deformed fluid escape pipes could be used as a large scale strain marker to constrain the flow regime during the time interval represented

by the pipe trail and computed a bulk viscosity for the salt sheet of 2.3×10^{18} Pa·s that is within the range derived from field and laboratory measurements for common evaporite minerals. These studies concluded that the deformed geometry of the fluid escape pipes through the salt revealed that the salt flow regime during Phase 2 was dominantly Couette (Figure 1) in this area of the translational domain. Since the shear strain related to this Couette flow regime can be accurately constrained, it should be possible to remove this latest strain imposed on the salt sheet during Phase 2 and to restore to the strain that resulted from Phase 1. This in turn would allow a direct comparison of the internal deformation in the final state, after Phase 1 and 2 deformation, with the state achieved after the initial Phase 1.

The aim of this paper therefore is to use this rationale of restoring the effects of the later Phase 2 Couette flow, to identify the true internal architecture of the salt following the initial Phase 1 of deformation. This is important because only then can future works conduct an informed investigation into the drivers for salt flow during Phase 1. We do this in the study area of the North Levant Basin where there is the independent constraint of internal kinematics during Phase 2 provided by the passive strain markers of the fluid escape pipe trails. Using the strain implied by the deformed fluid escape pipes, we restore the observed present day deformation of an area within the translational domain and remove the effects of the Phase 2 deformation, via 2D cross section and map restorations. We show that this restoration takes account of the strain in the salt sheet related to larger scale kinematics of the linked, updip gravity-driven extensional domain. The restored geometry at the onset of fluid escape pipe formation is revealed to be a much simpler gross deformational style than would be suspected had this restoration not been possible. This restored geometry is shown to have occurred in the Late Messinian, therefore clearly demonstrating in this area at least, a predominantly two phase deformational history, with substantially different flow regimes. This restoration method has wide implications for the analysis of multiphase deformation in all salt basins where there is coupling between salt flow and overburden response.

2 | GEOLOGICAL SETTING

The study area is located offshore Lebanon in the North Levant Basin (Figure 2a). The Levant Basin forms one of a series of linked basins in the Eastern Mediterranean that formed initially during Tethyan rifting, experienced prolonged regional subsidence in the Cretaceous to Miocene, punctuated by phases of regional folding (Syrian Arc deformation) in the Late Cretaceous, Eocene and later Neogene (Ben-Avraham, 1978; Gardosh & Druckman, 2006). A 1- to 2-km-thick unit of evaporites (Figure 2b) was deposited in

this region during the Messinian Salinity Crisis ca. 5.97 to 5.33 Ma (Krijgsman et al., 1999; Manzi et al., 2013; Meilijson et al., 2019; Ryan et al., 1973). The Messinian Evaporites reaches a maximum thickness to the southwest of the study area and thins to a pinch-out along a margin just seaward of the present day shelf edge (Figure 2b). The eastern flank of the basin was uplifted during the Late Neogene (Ghalayini et al., 2018; Nader, 2011), which is considered the dominant driver for the salt tectonic deformation of Phase 2 seen in the Pliocene to Recent overburden, with an updip extensional domain, a translational domain and a downdip contractional domain developed as a manifestation of classic gravity driven deformation (Figure 2b) (Cartwright & Jackson, 2008; Gradmann et al., 2005). Further south, deformation in the Levant Basin during Phase 2 is driven to varied amounts by a combination of basinward tilting of the margin and differential loading (Allen et al., 2016; Ben Zeev & Gvirtzman, 2020; Cartwright & Jackson, 2008; Gradmann et al., 2005; Zucker et al., 2020). An earlier Phase 1 of Late Messinian deformation was recognised by Netzeband et al. (2006) and Bertoni and Cartwright (2007) from the planation of intrasalt folds at a prominent truncation surface (the intra-Messinian Truncation Surface [IMTS], also represented by the Top Salt) (Figure 2b) (Gvirtzman et al., 2017; Kirkham et al., 2020). The driver for Phase 1 is poorly understood, but has been suggested to be basin tilting, via some combination of deep basin subsidence and marginal uplift (Bertoni & Cartwright, 2007; Feng et al., 2017; Gvirtzman et al., 2013; Kirkham et al., 2020).

The regionally correlatable internal reflectivity of the Messinian Evaporites has led to the subdivision of its stratigraphy in seismic reflection data into several intrasalt sequences named from the Base Salt upward as ME-I, ME-II, ME-III, ME-IV, ME-V and ME-VI (Figure 3). These are separated by intrasalt marker horizons named ME20, ME30, ME40, ME50 and ME60, as first outlined by Bertoni and Cartwright (2006) and Hübscher et al. (2007) (Figure 3). Other nomenclature used for these intrasalt sequences is summarised in Figure 3. The thin interbeds of diatomaceous claystones and claystones within the Messinian Evaporites (Meilijson et al., 2019) correlate with and are responsible for several discrete packages of high amplitude intrasalt reflections (ME20, ME-III and ME-V) that alternate with reflection free intervals (ME-I, ME-II, ME-IV and ME-VI; Figure 3). The immediate overburden to the salt consists of a latest Messinian clastic unit (interbedded with thin evaporites) of probable fluvial to shallow marine origin (the Nahr Menashe Unit (Madof et al., 2019); Figures 2b and 3). The Messinian sequence is overlain by shelf to slope sediments of Pliocene to Recent age (Figure 2b), deposited as the basin margin prograded basinwards after the rapid reflooding of the Mediterranean during the earliest Pliocene (Garcia-Castellanos et al., 2009; Ryan & Cita, 1978).

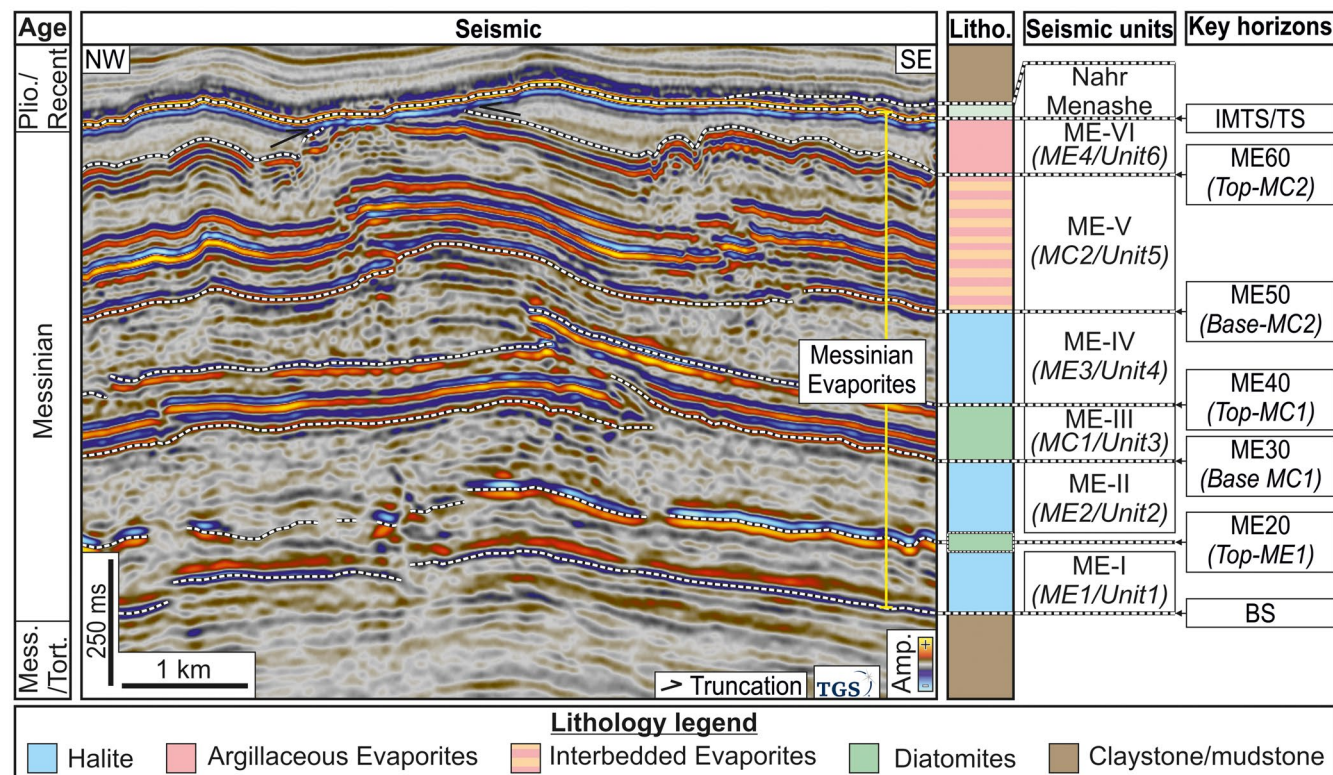


FIGURE 3 Stratigraphy of the Messinian Evaporites. A seismic profile showing the internal reflectivity within the Messinian Evaporites and truncation of intrasalt reflections at the intra-Messinian Truncation Surface (IMTS). The lithology (litho.) column includes information on the composition of the seismically reflective and transparent sequences in the Messinian Evaporites (from Meilijson et al., 2019) and the various nomenclature (compiled from Bertoni & Cartwright, 2007; Feng et al., 2016; Gvirtzman et al., 2017; Lofi et al., 2011; Lofi, 2018) for the seismic units and key horizons is outlined. Top Salt; BS, Base Salt. Seismic data courtesy of TGS [Colour figure can be viewed at wileyonlinelibrary.com]

3 | DATA AND METHODS

The 3D pre-stack time migrated seismic survey used in this study covers an area of 5,350 km² within the deep water off-shore Lebanon and has been provided by TGS. The data have been processed to a zero phase wavelet and is displayed with SEG normal polarity whereby an acoustically hard reflection from an increase in acoustic impedance appears as a positive amplitude (Brown, 2011). The bin spacing is 12.5 m, yielding a lateral resolution of ca. 25 m. Within the intervals of interest for this paper, the Pliocene to Recent and Messinian Evaporites, the vertical resolution is ca. 10 and ca. 40 m, respectively. Average p-wave velocities of 2,000 m/s for the Pliocene to Recent and 4,200 m/s for the Messinian Evaporites are used, as recorded from nearby wells in the South Levant Basin (Feng et al., 2016; Gardosh & Druckman, 2006).

Schlumberger's seismic interpretation software package Petrel was used for interpretation of the 3D seismic data. The key marker horizons of the Base Salt, ME20, ME30, ME40, ME50, ME60, the IMTS/Top Salt and Gelasian/Calabrian boundary (from Kirkham et al., 2019) have been mapped wherever present in the 3D seismic survey. These horizons were picked manually and autocorrelated to produce time structure maps that are used

to effectively identify faults and folds associated with flow and deformation of the Messinian Evaporites. Gaps in interpretation in the maps of ME20, ME30 and ME50 are the result of either localised breaks in reflection continuity or a complete loss of coherency. These maps in combination with seismic cross sections form the foundation of the structural interpretation of the Messinian Evaporites and intrasalt within the study area.

To examine the effect of the Phase 2 (Late Pliocene to Recent) deformation on the internal deformation of the salt sheet, we undertook cross-sectional and map restorations from two representative subareas within the southern sector of the study area (Figure 4; see Sections 4.4 and 4.5). These two subareas were selected for the proximity to the fluid escape pipe trails related to the Oceanus and Saida-Tyr presalt structures, with a position basinward from them and the salt flow direction interpreted (Cartwright et al., 2018; Kirkham et al., 2019), the completeness of the salt sequence without significant truncation at the Top Salt and clear and distinctive intrasalt deformations that can be mapped (Figure 4; subareas A and B, respectively). This allowed us to base the restoration on the strain within the salt constrained by the deformed fluid escape pipes, i.e., a simple shear deformation with translation of the Top Salt by 3.4 and 6 km (average for the four Saida-Tyr fluid escape pipe trails that

are closely spaced over a lateral distance of 4 km) in an approximately NW direction (Figure 1), for the Oceanus and Saida-Tyr trails respectively. The shear strains (γ) computed ($\gamma = \Delta x/L$) for these are 2.2 and 3.8, based on translation distances recorded for the Oceanus and Saida-Tyr fluid escape pipe trails (Δx ; 3.4 and 6 km respectively), and using present day thicknesses of the salt sheet in subareas A and B (L ; 1.55 and 1.58 km, respectively). We assume that the salt sheet did not thicken or thin during translation (cf. Albertz & Ings, 2012). This assumption is supported by the low strains recorded in the overburden in the southern region of the study area (typically less than 1%).

Seismic profiles (analysed in Section 4.4) were extracted from the 3D survey along arbitrary lines taken parallel to the flow direction implied by the fluid escape pipe trails (Figure 4). These

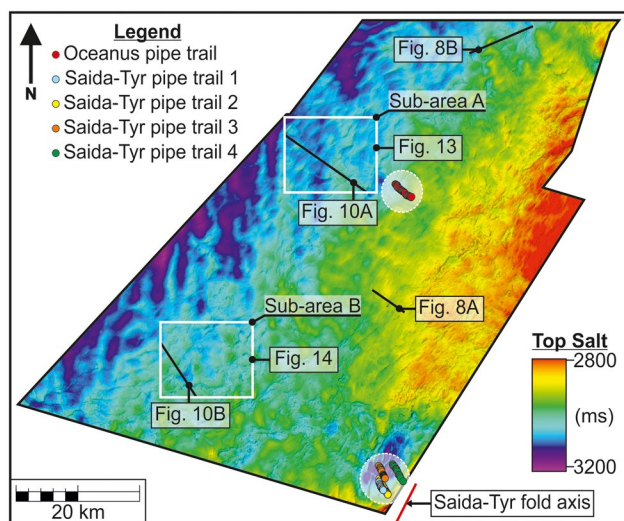


FIGURE 4 Map of the Top Salt that shows the locations of the Oceanus and Saida-Tyr fluid escape pipe trails, as well as the locations of subareas A and B [Colour figure can be viewed at wileyonlinelibrary.com]

were depth converted, displayed at true scale and restored by imposing a reverse simple shear transformation on the deformed region. Restoration of the profiles was undertaken to remove deformation of Phase 2, and hence reproduce the geometry of the internal markers extant at the end of the Messinian, at the time that the uppermost layers of salt were truncated at the IMTS following Phase 1 deformation. This critical step is illustrated graphically in Figure 5. The Corel Corporations vector graphics editing software package CorelDRAW X7 was used to undertake cross-sectional reconstruction, following Alsop et al. (2020). The key marker horizons within seismic cross section were traced within the software and then deformed by simple shear using the skew tool (see Figure S1).

The primary assumptions driving this cross-sectional 2D restoration is that the strain within the salt sheet was ideal Couette (as interpreted from the fluid escape pipe trails in Cartwright et al., 2018; Kirkham et al., 2019), with a constant shear strain vertically through the sheet, with intrasalt layers acting as passive markers with no mechanical competency. The recent well calibration of the intrasalt reflections to thin (1–4 m) layers of claystone and diatomite interbedded within an almost pure halite sequence (Feng et al., 2016; Meilijson et al., 2019) does not convey any need to consider these thin layers as being mechanically significant. It is conceivable that rapid burial and loading of these thin layers by the dominantly halite unit that hosts them impeded dewatering and resulted in undercompaction and overpressure (Osborne & Swarbrick, 1997). In an attempt to independently evaluate the validity of this assumption, we attempted map based restorations of subareas A and B (see Section 4.5). The method applied was to restore structural maps of Base Salt, ME20, ME30 and ME50 using translation vectors derived from the fluid escape pipe trails, and with reduction in translation distance proportionately downwards to the Base Salt according to the shear strain calculated for each subarea. The aim is to

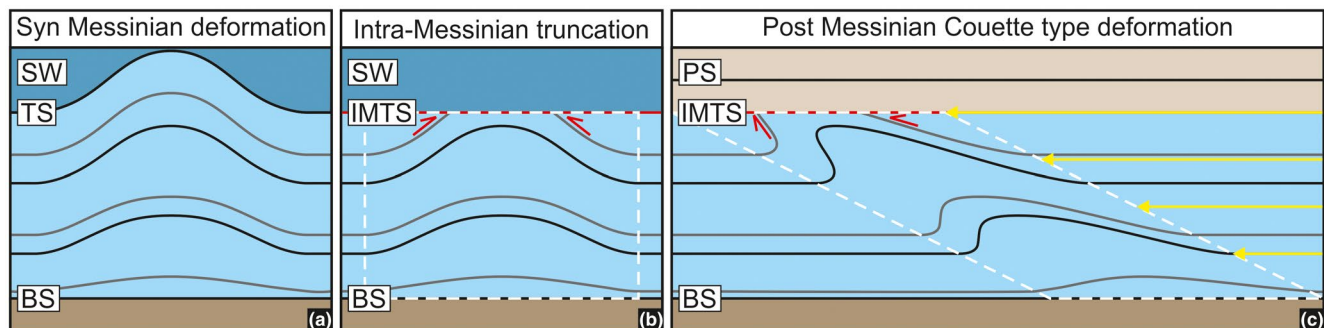


FIGURE 5 A sequential illustration to demonstrate the impact of a Couette-type flow deforming the Messinian Evaporites in the study area from the Late Pliocene to Recent. (a) The Messinian Evaporites and its intrasalt layers are folded during the Late Messinian phase of deformation (Gvirtzman et al., 2013). (b) The upper section of the Messinian Evaporites are removed during the intra-Messinian dissolution and truncation event (Kirkham et al., 2020). (c) The already folded intra-salt layers in the Messinian Evaporites are deformed further by Couette flow (simple shear; represented by the yellow arrows and dashed white box), recorded first by the Oceanus fluid escape pipe trail (Cartwright et al., 2018). BS, Base Salt; IMTS, intra-Messinian Truncation Surface; PS, post-Salt; SW, Seawater; TS, Top Salt [Colour figure can be viewed at wileyonlinelibrary.com]

restore the structures within the maps to their original position post-Phase 1 deformation but prior to Phase 2 deformation.

4 | RESULTS

4.1 | Overview of structure of the study area

The study area is characterised by a fairly smooth and flat-lying Base Salt geometry at a regional scale, with localised folding of this surface into upright anticlines with a few hundred metres amplitude, 5- to 10-km wavelengths, and fold axes trending NNE-SSW (Figure 6a). The location of the Oceanus and Saida-Tyr pre-salt folds, from which the Oceanus and Saida-Tyr fluid escape pipe trails are sourced, is shown in Figure 6a. These structures are part of the regional Syrian Arc deformational system (Nader, 2011). A regionally extensive set of dominantly WNW-ESE striking extensional faults with a spacing of a few kilometres (throws typically

10 s to a few 100 m) occur within the Eocene to Miocene succession (Figures 6a and 7). These faults detach in the Upper Eocene and extend upwards to offset the Base Salt, before tipping out within the lowermost units of the Messinian Evaporites (Figure 7). They have been extensively described by Ghalayini et al. (2017) and Reiche et al. (2014).

The salt sheet maintains an almost uniform thickness of 1.5 km over the western part of the study area but thins towards a pinch-out located near the present coastline, east of the study area (Figure 2). A coast-parallel 10- to 20-km-wide zone of extensional faults extends along the length of this eastern margin of the Levant Basin (Cartwright & Jackson, 2008; Elfassi et al., 2019; Kirkham et al., 2019). This fault array defines the extensional domain (Figure 2b), striking parallel to the basin margin, dipping predominantly basinward, with throws of tens to hundreds of metres. Growth on these faults occurred from the Late Pliocene onwards, a similar timing to that documented further south (Cartwright & Jackson, 2008; Elfassi et al., 2019). The Top Salt is also relatively un-deformed, except in the extensional domain

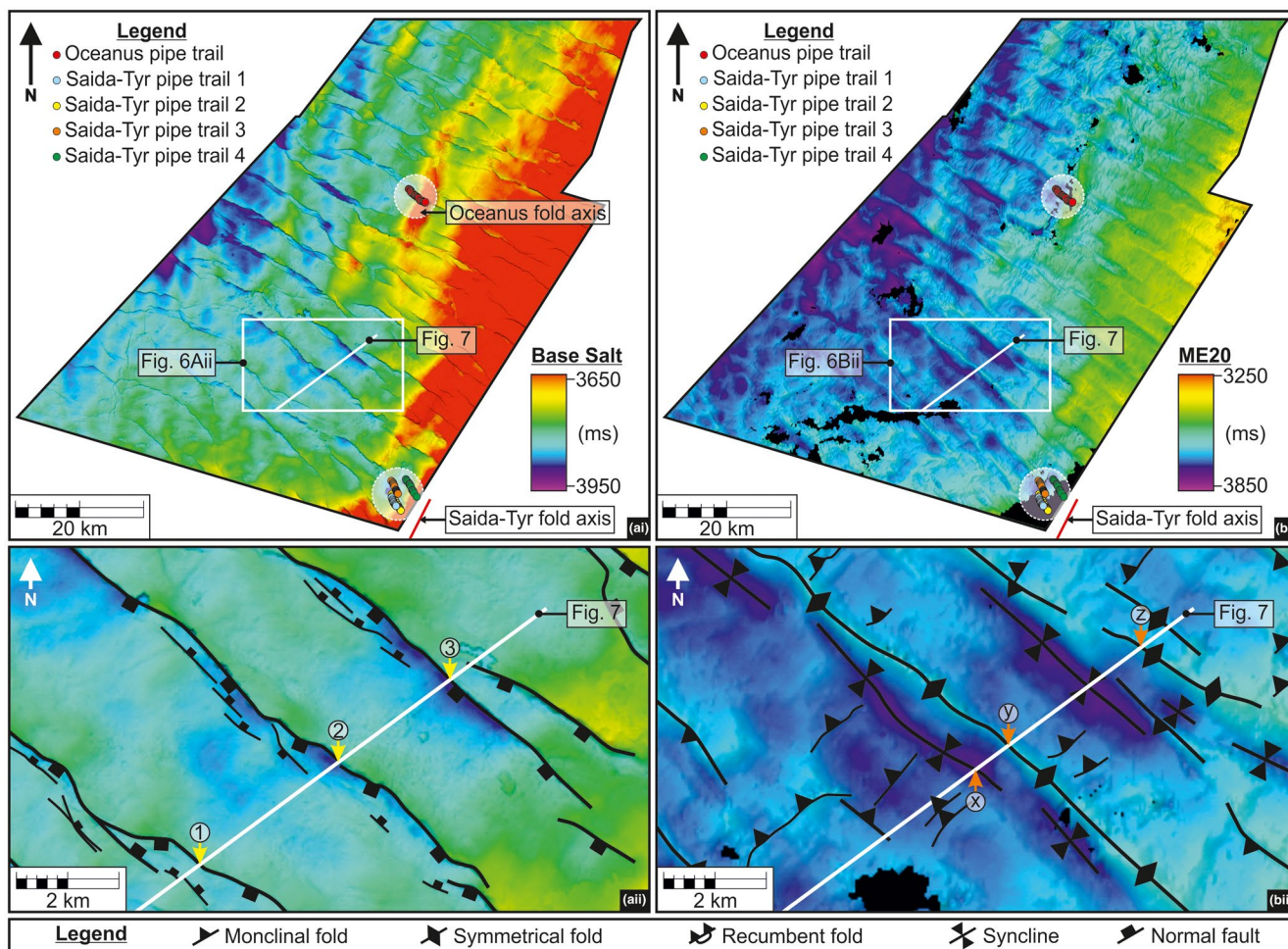


FIGURE 6 Structure maps of the Base Salt and ME20 within the 3D seismic study area, with the locations of the Oceanus and Saida-Tyr fold axis' and fluid escape pipe trails. (Ai and Aii) A map of the Base Salt that is dominated by WNW-ESE normal faults and NNE-SSW folds. The numbered faults 1, 2 & 3 correlate with faults in Figure 7. (Bi and Bii) A map of ME20 showing synclines and anticlines that are oriented WNW-ESE similar to the normal faults at the Base Salt as well as other minor folds verging NW. The folds x, y and z correlate with folds in Figure 7 [Colour figure can be viewed at wileyonlinelibrary.com]

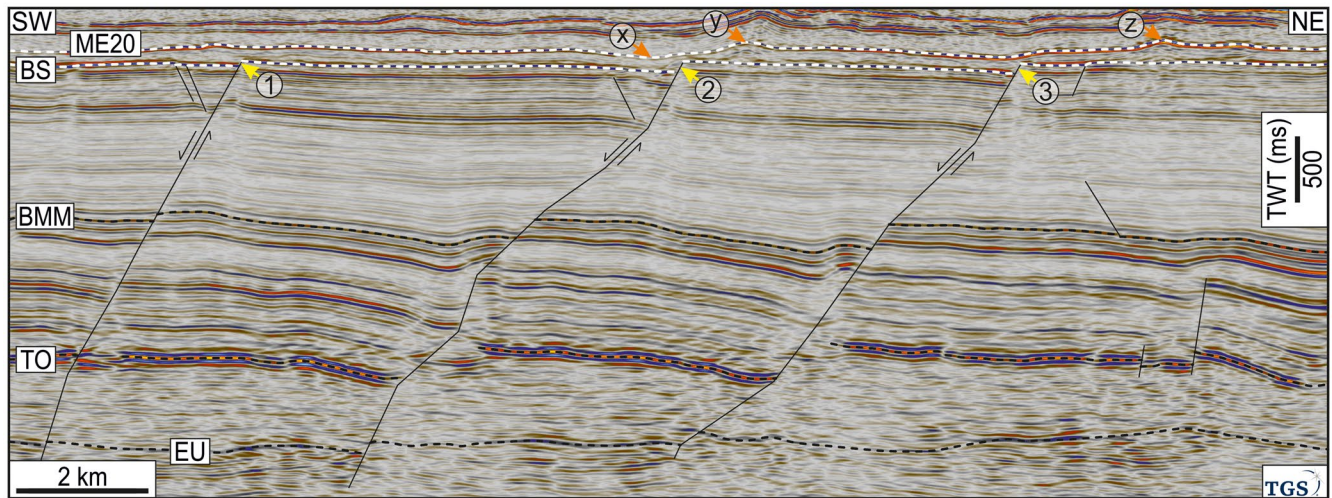


FIGURE 7 Pre-salt faults that detach in the Eocene and extend upward to the Base Salt (BS) (see Figure 6 for line location). The lower intra-salt reflection of ME20 is folded overlying the pre-salt faults. The structure labelled numbers 1, 2 and 3 and letters x, y and z correlate with structures in the maps in Figure 6a,b, respectively. BMM, Base Mid-Miocene; EU, Eocene Unconformity; TO, Top Oligocene. Seismic data courtesy of TGS [Colour figure can be viewed at wileyonlinelibrary.com]

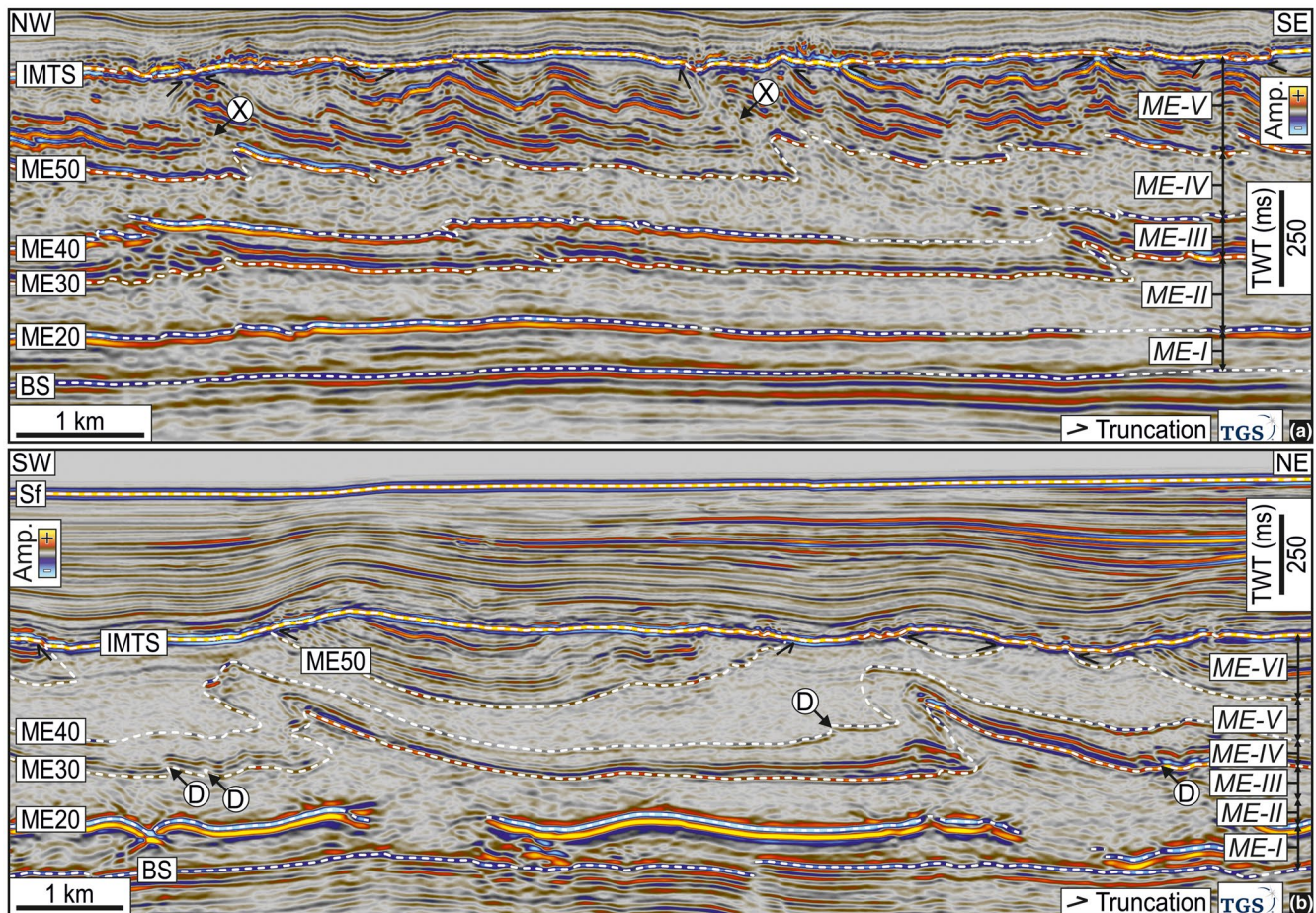


FIGURE 8 The style of deformation within the Messinian Evaporites (see Figure 4 for seismic profile locations). (a) A seismic profile that highlights the greater deformation within the Messinian Evaporites in contrast to the weakly deformed layers overlying the intra-Messinian Truncation Surface (IMTS). The reflections of sub unit ME-V are heavily truncated at the IMTS. Coherency is lost in some folds (as highlighted by labels X) where there are large and abrupt changes in dip. (b) A seismic profile showing two clearly recumbent folds in sub unit ME-IV. Folding of ME30 and ME40 is harmonic, with disharmony only in small structures (as highlighted in labels D). BS, Base Salt; Sf, Seafloor. Seismic data courtesy of TGS [Colour figure can be viewed at wileyonlinelibrary.com]

and also further west, where a swath of minor, almost symmetrical folds is mapped at Top Salt (Figures 2b and 4; see Figure 1b in both Cartwright et al., 2018; Kirkham et al., 2019). These folds have wavelengths of 2–4 km, NNE striking axial planes, are periclinal in three dimensions with maximum amplitudes of <100 m. This array of minor folds defines the limits of the contractional domain (Figure 2b). The study area is delimited to the north by the NE-SW striking Latakia Ridge (Figure 2a) (Hall et al., 2005; Maillard et al., 2011), and the intensity of these overburden folds increases with proximity to this major structure.

In contrast to the relatively weakly deformed Top Salt and overburden, the salt sheet is highly deformed internally almost exclusively by contractional structures, which are predominantly truncated at the IMTS (Figure 8a). Only rarely is there any significant structural continuity from within the deformed salt into the lesser deformed overburden. The contractional structures exhibit a large range in geometry and orientation, laterally and vertically, and are described in detail below.

4.2 | Internal structure of the Messinian Evaporites

The internal structure of the Messinian Evaporites is mappable over the entire study area due to the high lateral continuity and high amplitude/frequency character of the internal reflections. The imaging of the intrasalt multilayers is excellent in general, but there is some loss of amplitude and coherence wherever there are abrupt and large magnitude changes of dip (see labels X in Figure 8a). This is acute on the lower limbs of overturned folds, particularly close to the crestal line. The time migration has resulted in well-imaged structures that map consistently along strike with often subtle changes in geometry recorded over short spatial intervals. The internal structure is described in detail below using horizon maps of the most laterally continuous, reflective intrasalt markers, ME20, ME30 and ME50. Since the uppermost salt units are truncated at the IMTS over most of the north-eastern part of the study area, the description focuses on the southern sector of the study area (Figure 4) where the most complete salt stratigraphy is preserved.

4.3 | Structural description of the intrasalt layers

The structure of the area varies considerably both laterally and vertically. Structural style close to the base of the salt sheet is best seen in the map of ME20 (Figure 6b) and is dominated by the synclines and upper tip monoclinical and upright folds of the WNW-ESE trending normal faults at the Base Salt (Figure 6a) described by (Ghalayini et al., 2017). Minor asymmetric folding is also seen, with a general vergence towards the NW

(Figure 6b), but of much lower amplitude than that visible at shallower levels within the salt (Figure 7). The majority of these minor folds die out beneath ME30, within the non-reflective interval ME-II. Only rarely are folds at ME20, typically NW-SE upright folds, observed to link with structures at ME30 or above, and hence a detachment is inferred within ME-II (cf. Cartwright et al., 2012; Gvirtzman et al., 2013).

The structure in the central part of the salt layer (ME-III) is characterised by a range of fold types, from recumbent to monoclinical and upright, with a range of fold axis orientations (Figure 9a). The recumbent and monoclinical folds typically verge towards the NW (Figure 10), but a minority verge to the west or north. Upright symmetric folds are predominantly oriented SE-NW. Fold relief is typically 100–300 m within this central region and fold limb dips are in the range 11°–25°. Fold axis lengths are of the order of 1–8 km, and the variably oriented structures sometimes intersect each other with no systematic offsetting of one trend over another. In addition to the obvious folds, there are many smaller structures of more cryptic origin with generally minor amplitude or displacement. These closely resemble reverse shear zones described within the Aptian Salt of the Santos Basin by Jackson et al. (2015) and are therefore interpreted similarly here. These shear zones typically verge NW, occur in clusters and are often more closely spaced than the larger amplitude folds (Figures 8–10). Some of these reverse shear zones change in their geometry along strike to become more obviously recumbent folds, and there is evidently a gradation between these two structural styles with increasing displacement. Seismic profiles show that ME30 and ME40 are deformed harmonically throughout the study area (Figure 8b), with disharmony only in minor folds (see labels D in Figure 8b), implying that only small structures detach between these two horizons.

The structures seen at the shallowest levels (ME-V) within the salt sheet exhibit the same geometrical variation and intersection relationships as those seen in the centre (ME-III) of the sheet (Figure 9b) but are consistently offset laterally from those at deeper levels, suggesting that a significant detachment occurs in ME-IV. The amplitude of the folds mapped at ME50 is considerably larger than those mapped at ME30, typically ranging from 100 to 500 m. Fold spacing is closer too (typically 1–2 km), with a larger number of smaller scale reverse shear zones and recumbent folds than seen at deeper levels. The deformational intensity thus is apparently greatest near the top of the salt layer, diminishing with depth through the salt sheet, and with two major detachments occurring in the thickest of the non-reflective intervals (ME-II and ME-IV).

4.4 | Structural restoration

Representative examples of the restorations from the two subareas are shown in Figures 11 and 12, showing the initial

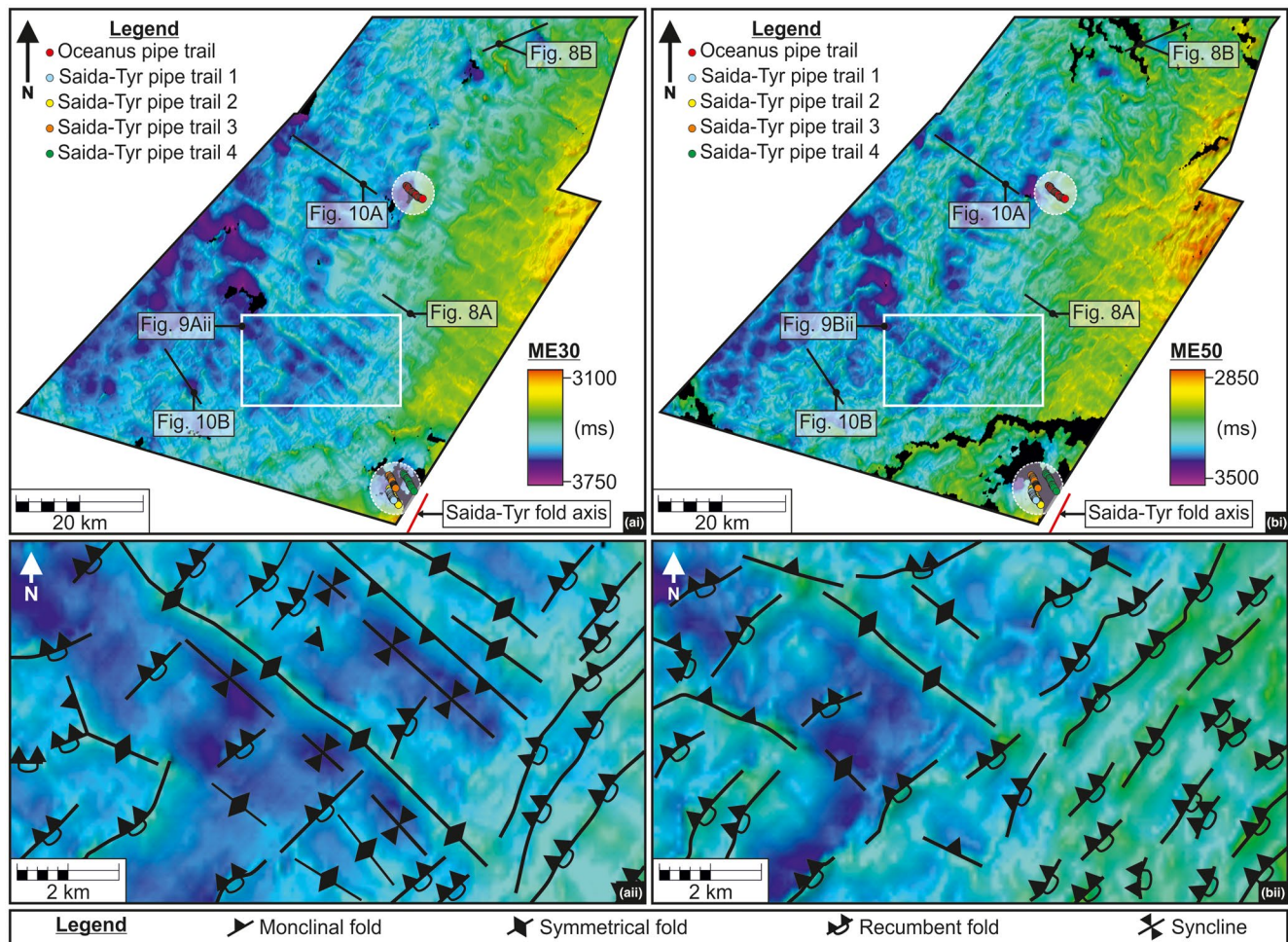


FIGURE 9 Structure maps of ME30 and ME50. (Ai and Aii) A map of ME30 showing that the horizon is characterized by upright, monoclinical and recumbent folds. The upright folds are dominantly oriented NW-SE while the monoclinical and recumbent folds predominantly verge NW. (Bi and Bii): A map of ME50, showing a similar structural style to ME30, but with fewer upright folds and a greater dominance of recumbent folds [Colour figure can be viewed at wileyonlinelibrary.com]

and final geometry before and after restoration (see Section 3 for method). The unrestored profile 1 from subarea A (Figure 11a) is typical of the structural style visible in the NW flow direction. The general NW vergence of most of the structures is evident at all the reflective marker horizons, as is the apparent detachment between ME20 and ME30, and between ME40 and ME50 (Figure 10a). The geometry of the recumbent folds in ME30/40 is clearly imaged, with axial planes dipping at ca. 17° to the SE, and upper limbs showing thinning between ME30 and ME40. The upward continuation of these folds into the uppermost salt layers is not imaged, and there is marked truncation of these structures at the IMTS. Numerous reverse shear zones are evident at all levels within the salt but cannot be traced continuously across the thick non-reflective layers of ME-II and ME-IV. If we make a standard assumption of conservation of line length of the individual reflective marker horizons, a classical line length balancing method to compute the apparent shortening represented in this unrestored section can be used (Fossen, 2016;

Chapters 20 and 21). With this assumption, the unrestored profile exhibits shortening from a low value of 8% at ME20, to 18% at ME30, 20% at ME40 and 19% at ME50, showing a general upward increase in shortening but with the greatest shortening recorded at ME40. An upward increase in shortening has been observed in previous studies on unrestored profiles conducted further south in the basin (Cartwright et al., 2012; Feng et al., 2017).

Application of a retro-shear (Figure 5 and Figure S1) leads to the reconstruction of the restored profile 1 (Figure 11b) which dramatically contrasts with the unrestored geometry (Figure 11a). The recumbent folds have been systematically restored from their highly overturned aspect into upright folds, with approximately vertical axial planes. The smaller, reverse shear zones are present as asymmetric kinks or steps in the layering, with vertical offsets identical to those seen in the unrestored profile, but with a kink axis that is almost vertical. Truncation angles between the uppermost reflective layers and the IMTS are noticeably different, but because

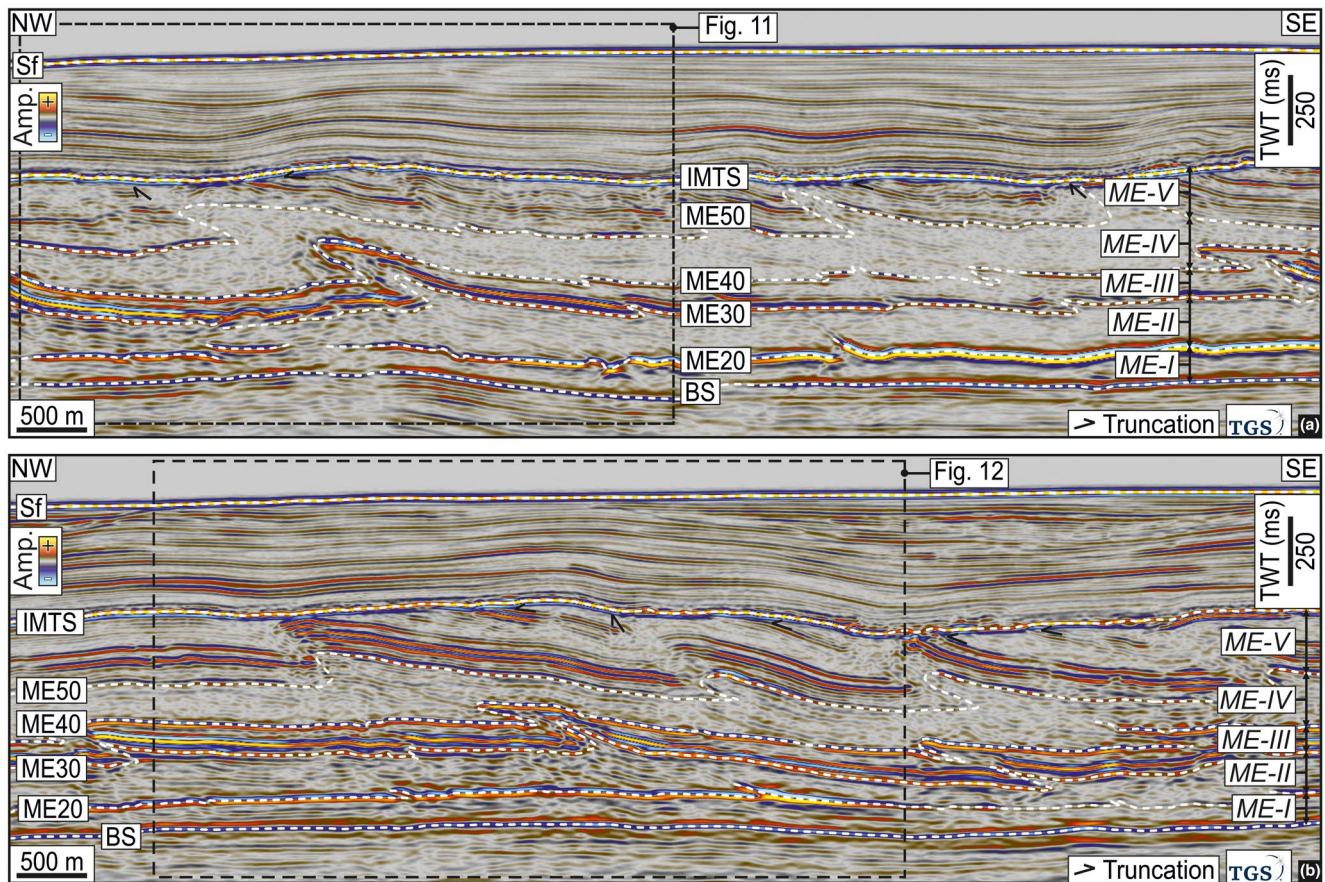


FIGURE 10 Cross sections oriented parallel to the recent salt flow direction in sub-area A and sub-area B (see Figures 4 and 9ai, Bi for line locations). These cross sections are dominated by recumbent and monoclinial folds with a vergence in the present day flow direction at all intra-salt layers ME20–ME50. There is an apparent detachment for these folds in ME-II and ME-IV. (a) A flow parallel seismic profile from subarea A. The dashed box highlights the section that is retro-sheared in Figure 11. (b) A flow parallel seismic profile from subarea B. The dashed box highlights the section that is retro-sheared in Figure 12. BS, Base Salt; IMTS, intra-Messinian Truncation Surface; Sf, Seafloor. Seismic data courtesy of TGS [Colour figure can be viewed at wileyonlinelibrary.com]

the overburden is coupled to the Top Salt, the distances between successive truncated markers are identical in the restored and unrestored profiles (e.g., points X–X' and Y–Y' on Figure 11a,b). Most interestingly, structures from different levels within the salt that were widely separated originally, now align almost vertically once the retro-shear has been applied (Figure 11b).

The unrestored profile 2 located in subarea B (Figure 12a) shows similar patterns of internal deformation and geometry of individual structures to profile 1 (Figure 11a). The vergence of all the seismically visible structures is to the NW, with a mixture of fold styles from recumbent with tightly isoclinal hinges to more open, asymmetric forms (Figure 10b). The amplitude of the folds is noticeably larger at ME50 compared to ME40, and there is a closer spacing of structures at the upper level. Axial planes are typically in the 15°–25° range. It is possible to connect structures from ME40 to ME50 by projecting along this general dip in the direction of general NW vergence, such that it is not obvious that a detachment exists between these two layers. Line balancing yields an

upward increase in the value of shortening represented by the deformed marker horizons, although the upward increase is less marked than for profile 1, and with slightly higher values recorded at ME20 (12%) and ME30 (15%) and the same value recorded from ME40 and ME50 (16%; Figures 10b and 12a).

The restored geometry of profile 2 (Figure 12b) is again strikingly different from its unrestored counterpart. The highly recumbent folds restore to upright folds with open hinges and vertical axial planes, to folds with a slight vergence to the SE in the opposing direction to their present day vergence. This opposite vergence may be removed had a less translation distance of for example ~5 km been used and perhaps reflects minor error in utilising an average translation distance from the four closely spaced Saida-Tyr fluid escape pipe trails. As with profile 1, the retro-shear also results in re-alignment of the structures seen at different marker horizons, such that widely separated structures have been translated into a more vertical alignment.

The changes in geometry shown for the two restorations presented in Figures 11 and 12 are typical for all restorations constructed on profiles aligned with the local salt flow

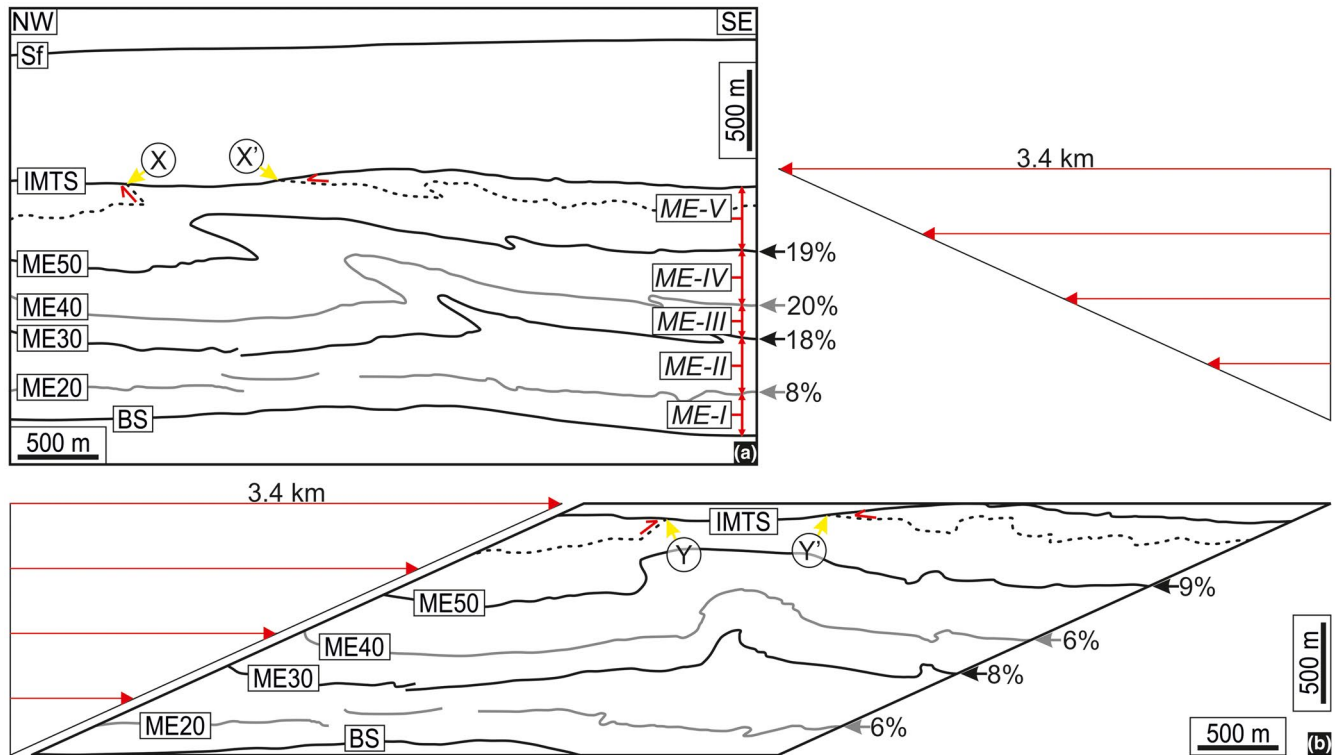


FIGURE 11 Retro-shear restoration of a cross section (profile 1) parallel to the strike of the Oceanus fluid escape pipe trail and % shortening for ME20-ME60. (a) An extraction and depth conversion of the key marker horizons from the flow parallel seismic profile in Figure 10a from subarea A (Figure 4). The intra-salt layers are characterized by NW verging monoclinical and recumbent folds. This present day geometrical configuration of intrasalt horizons follows a simple shear of the Messinian Evaporites with 3.4 km of translation of the Top Salt, as recorded from the nearby Oceanus fluid escape pipes trail. (b) A restoration of the profile in Figure 11a after retro-shearing the Messinian Evaporites, to remove the effect of the Late Pliocene to Recent simple shear and 3.4 km translation of the top salt. As a result, the folds in the intrasalt layers have become more upright and display a vertical stacking. BS, Base Salt; IMTS, intra-Messinian Truncation Surface; Sf, Seafloor [Colour figure can be viewed at wileyonlinelibrary.com]

direction. We find consistently that any recumbent folds striking approximately NE-SW restore to an upright to sub-upright fold geometry with reduced limb dips compared to the unrestored precursor. From this, we conclude that NE-SW striking recumbent folds in the study area most likely formed by the Phase 2 simple shear of originally almost upright folds that formed during Phase 1. Interestingly, the rotation of the axial planes of these early formed folds from their upright position closely matches the rotation required by the shear strain implied by the once vertical and now deformed fluid escape pipe trails in the salt. It is harder to be sure about the restored geometry of tightly isoclinal structures and the smaller reverse shear zones. These restore to unusual geometries characterised by steep limbs and modest interlimb angles. It is possible that seismic imaging of these smaller structures is not as reliable as it is for the larger structures, because seismic migration is more error prone as the limit of spatial resolution is approached (Berkhout, 1984), or they represent some minor uncertainty in the restoration method.

Shortening calculations made with the standard approach of line length balancing were applied to the restored sections, to gauge the level of deformation and the vertical strain

distribution that accrued during Phase 1 deformation. The values of shortening for all the key marker horizons show a marked difference with those computed from the unrestored sections by a factor of between 2 and 4 (computed values in Figures 11a,b and 12a,b). In addition, the vertical strain distribution does not show much of an upwards variation, certainly, nothing comparable to this computed for the unrestored profiles. The validity or otherwise of these shortening values in restored or unrestored states is considered in detail in Section 5.

4.5 | Map restoration

The 2D profile restorations demonstrate the effect of removing the internal strain of the salt sheet that accrued during Phase 2 deformation in this part of the Levant Basin. We look to further validate this approach via map restorations (see Section 3 for method). We mapped all of the faults at Base Salt and folds at ME20, ME30 and ME50 within subareas A and B (Figures 13 and 14), spaced ~30 km apart (Figure 4). One of the characteristics of the folds in the central (ME-III) and upper parts (ME-V)

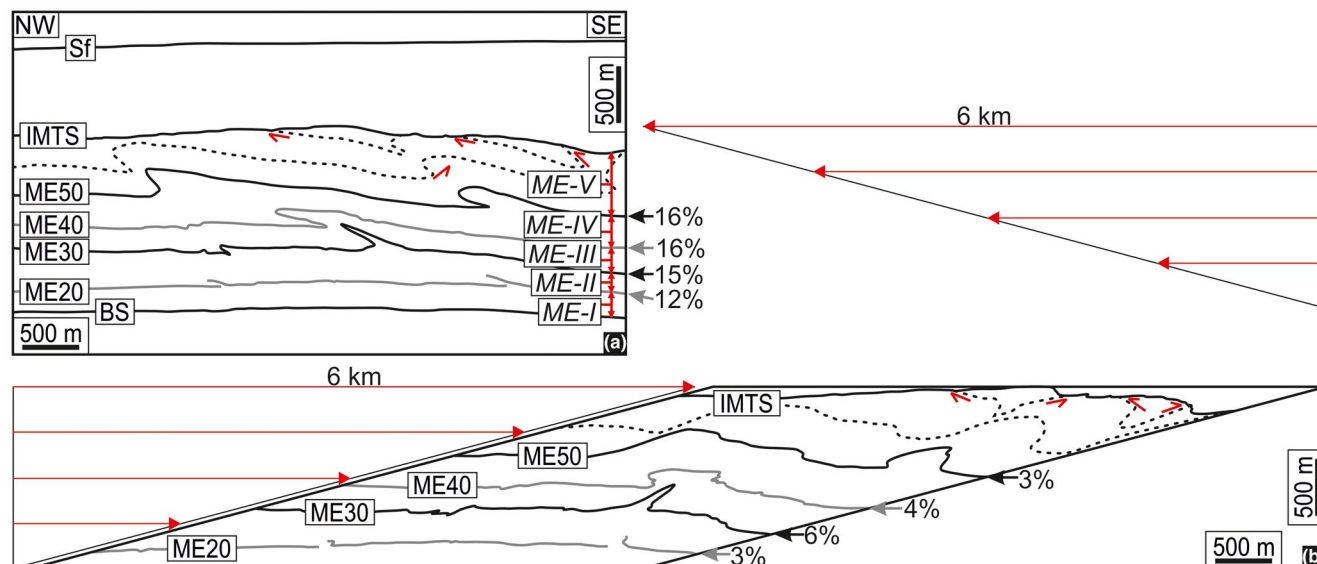


FIGURE 12 Retro-shear restoration of a cross section (profile 2) parallel to the strike of the Saida-Tyr fluid escape pipe trails and % shortening for ME20-ME60. (a) An extraction and depth conversion of the key marker horizons from the flow parallel seismic profile in Figure 10b from subarea B (Figure 4). This present day geometrical configuration of intrasalt horizons follows a simple shear of the Messinian Evaporites with ~6 km of translation of the Top Salt, as recorded from the nearby Saida-Tyr fluid escape pipe trails. (b) A restoration of the profile in Figure 12a after retro-shearing the Messinian evaporites, to remove the effect of the Late Pliocene to Recent simple shear and ~6 km translation of the Top Salt. As a result, the folds in the intrasalt layers have become more upright to sub-upright and show a greater vertical stacking and slight vergence SE. BS, Base Salt; IMTS, intra-Messinian Truncation Surface; Sf, Seafloor [Colour figure can be viewed at wileyonlinelibrary.com]

of the salt sheet is their range of fold axial orientations over small areas. Coupled with the tendency for some of these folds to intersect at high angles, the overall organisation of the folds is distinctive although somewhat puzzling too, in the broader context of salt deformation (see Section 5). It was therefore hoped that restoration of fold axes would move the fold axis within the intrasalt layers back to their original post-Phase 1 position prior to Phase 2 and would allow some insights into the folding style developed from Phase 1 that are currently concealed by the superposition of the later Phase 2 deformation.

Subarea A is characterised by folds with linear to curvilinear axes oriented NE-SW, NW-SE and E-W at all the marker horizons. The major synclines and anticlines at ME20 are oriented NW-SE and vertically align with the NW-SE oriented normal faults at the Base Salt once translated to their original post-Phase 1 position (Figure 15), indicating that much of the structure at ME20 is governed by pre-salt deformation. With the exception of the near overlapping synclines labelled S in Figure 16a, the major folds at ME20, as well as the numerous minor dominantly NE-SW monoclinical and upright folds, are not correlatable with the folds at ME30 following retro-shearing. The principal fold axes for ME30 and ME50 show similar gross patterns of folding predominantly oriented NE-SW but with progressive offsetting of these axes in a north-westerly direction (Figure 13c,d). Simple retro-shearing of this set of maps by values derived from the Oceanus fluid escape pipe trail results in these structures becoming vertically aligned, with a high

degree of conformity in gross fold planform for the restored individual surfaces (see examples labelled T in Figure 16b). The mapped structures in ME30 and ME50 that do not realign following retro-shearing (see label R in Figure 16b) are typically of smaller scale and appear to detach within ME-IV.

A similar map restoration using values derived from the Saida-Tyr fluid escape pipe trails (6 km of translation and a Couette flow profile) was performed for subarea B and yielded a strikingly similar result (Figures 15b and 16c,d). Fold axes with similar lengths and detailed fold axis curvature but that were originally offset by as much as 5 km from each other from ME20 to ME50 are restored into near vertical stacking alignments (see examples labelled T' in Figure 16d). By contrast with subarea A, once retro-sheared a few major folds in ME20 and ME30 (labelled S' in Figure 16c) show geometrical similarities and appear closely aligned vertically, however, most detach within ME-II.

Although these map restorations do not prove uniquely that the internal strain of the salt sheet can be represented by a Couette flow kinematic profile through the salt, the striking alignment of similarly oriented structures and intersections lends strong support for this conclusion. In addition to aligning vertically, the structure types in the maps from substudies A and B would be modified once retro-sheared, as demonstrated by the 2D restorations (Figures 11 and 12). The recumbent folds in the ME30 and ME50 (e.g., T and T' in Figure 16b,d respectively) are therefore, likely to have been aligned and upright to

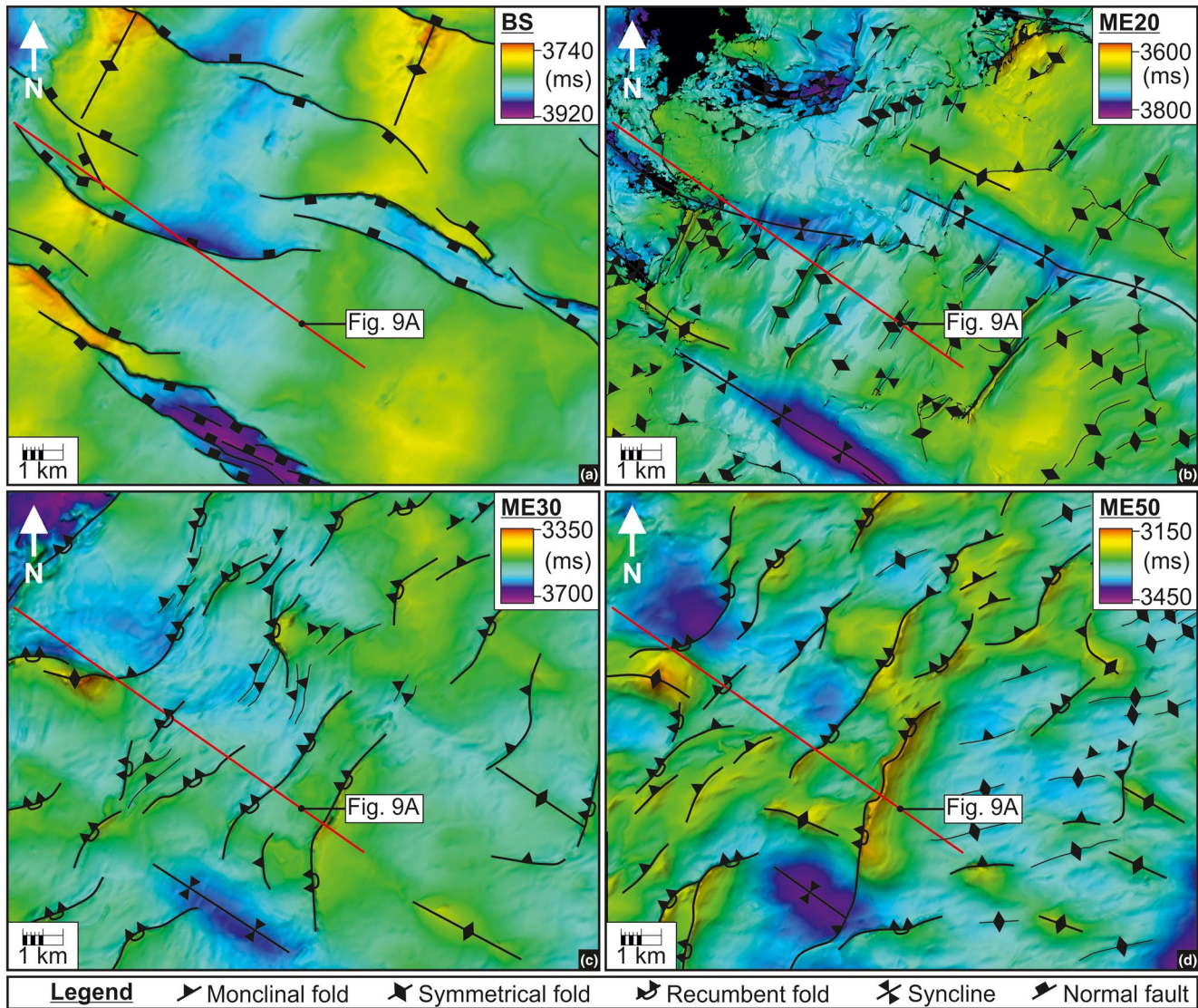


FIGURE 13 Structure maps in subarea A, located basinward of the Oceanus fluid escape pipe trail (see Figure 4 for location; thick lines = major structures; thin line = minor structures). (a) A Base Salt map structurally dominated by NW-SE oriented normal faults. (b) A map of ME20, characterised by NW-SW synclines and anticlines and minor NE-SW symmetrical folds. (c) A map of ME30 with dominantly NW verging recumbent folds and monoclines, as well as few NW-SE symmetrical folds and synclines. (d) A map of ME50 with a similar structural character to ME30, as well as and some minor E-W symmetrical folds [Colour figure can be viewed at wileyonlinelibrary.com]

subupright folds prior to imposition of a simple shear during the Phase 2 deformation of the Messinian Evaporites.

5 | DISCUSSION

5.1 | Multiphase deformation of the Messinian Evaporites

The continuity and clarity of the intra-Messinian seismic reflections over large areas of the Eastern Mediterranean presents a prime opportunity to analyse the internal kinematics of a deformed salt sheet (Hübscher et al., 2007). Here, we have extended the approach adopted in previous studies of mapping

the internal strain expressed in discrete structures such as folds and shear zones (see review by Rowan et al., 2019), by adding in the capability to retro-deform the salt using constraints from passive strain markers (the fluid escape pipes first described by Cartwright et al., 2018; Kirkham et al., 2019) and hence remove the effects of the latest phase of deformation to reveal the true strain developed during earlier phases of deformation.

Although there has been considerable debate over the question of how many phases of deformation the Messinian Evaporites have been subjected to, and when and why these occurred, most recent work supports the model initially proposed by Bertoni and Cartwright (2007) of regional pre-Pliocene (syn-Messinian) deformation (Gvirtzman et al., 2013; Kirkham et al., 2020; Netzeband et al., 2006),

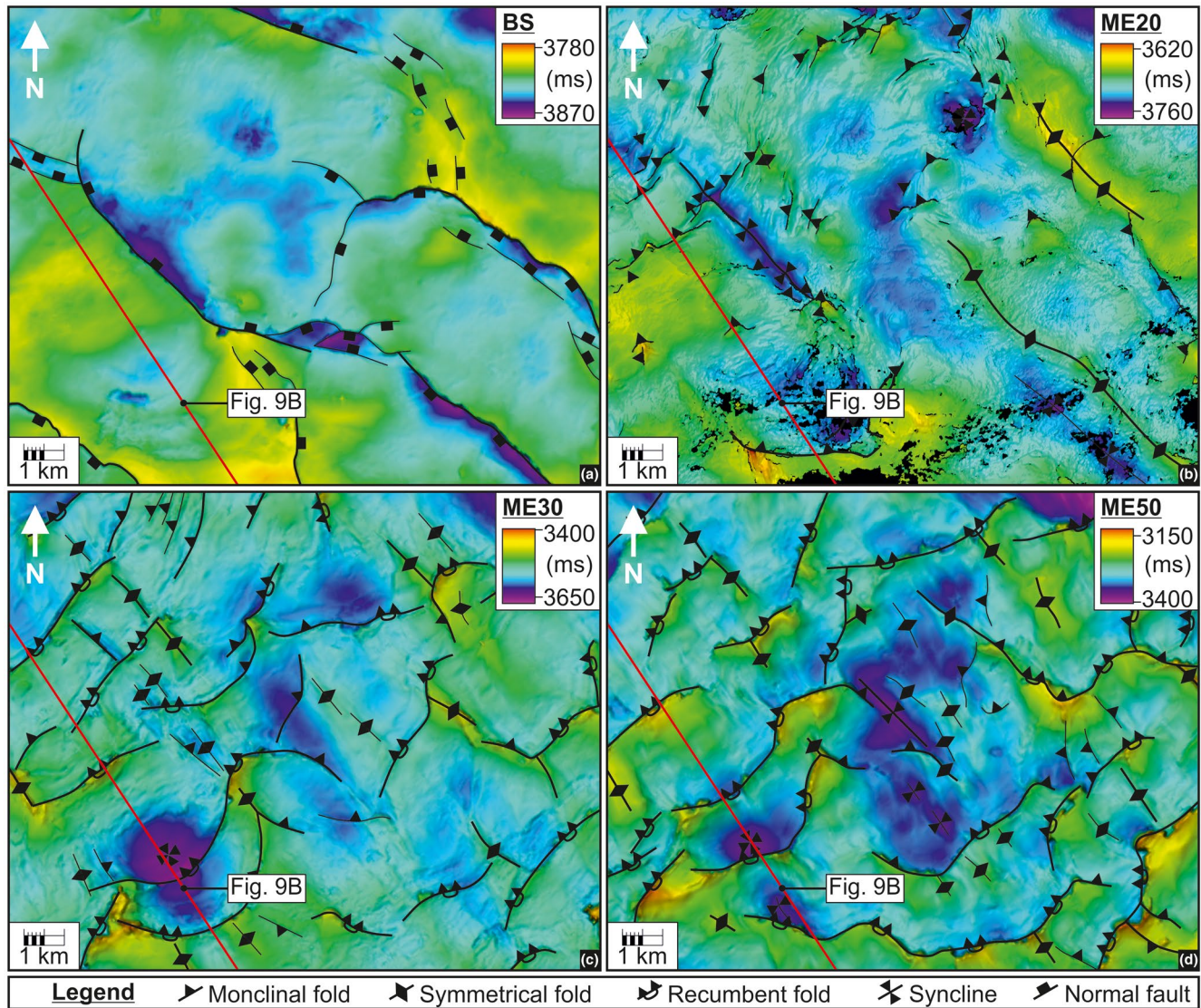


FIGURE 14 Structure maps in subarea B, located basinward of the Saida-Tyr fluid escape pipe trail (see Figure 4 for location; thick lines major structures; thin line = minor structures). (a) A Base Salt map showing normal fault oriented predominantly NW-SE, as well as few with a curved geometry. (b) A map of ME20 with NW-SW synclines and anticlines and minor NE-SW monoclinal folds. (c) A map of ME30 that is characterized by NW verging recumbent and monoclinal folds and few NW-SE symmetrical folds and synclines, with some distinct intersections between the different fold types. (d) A map of ME50 with a similar structural character to ME30, as well as the distinct structural intersections [Colour figure can be viewed at wileyonlinelibrary.com]

followed by an Early-Mid Pliocene quiescent period (Elfassi et al., 2019), and then a second phase in the Later Pliocene to Recent (Ben Zeev & Gvirtzman, 2020; Cartwright & Jackson, 2008; Elfassi et al., 2019). This two phase model is also fully supported by the results of this study, in which we show that retro-deformation of the salt to account for the Late Pliocene to Recent phase does not remove all the internal strain: far from it, the restored maps and profiles instead reveal a simpler style of internal folding than would be apparent if it was tacitly assumed that all the folding accrued in a single phase.

The limited restorations that we have undertaken to date all show that removing the effects of a later, superimposed

Couette flow profile (Phase 2 deformation) results in a more generally upright fold geometry with near vertical axial planes (Figures 11 and 12). The Couette flow profile interpreted from the deformed linear fluid escape pipe trails (Cartwright et al., 2018; Kirkham et al., 2019) matches the flow profile expected for salt deforming via gravity gliding (Albertz & Ings, 2012; Brun & Merle, 1985; Peel, 2014), which is in keeping with the model of marginal uplift and basin tilting (Bar et al., 2016; Elfassi et al., 2019; Ghalayini et al., 2018; Kirkham et al., 2019) as the primary driver for basinward salt flow in this part of the basin during Phase 2 deformation. These restored fold profiles show no strong vergence across the area, and no strong preferred shortening direction. This

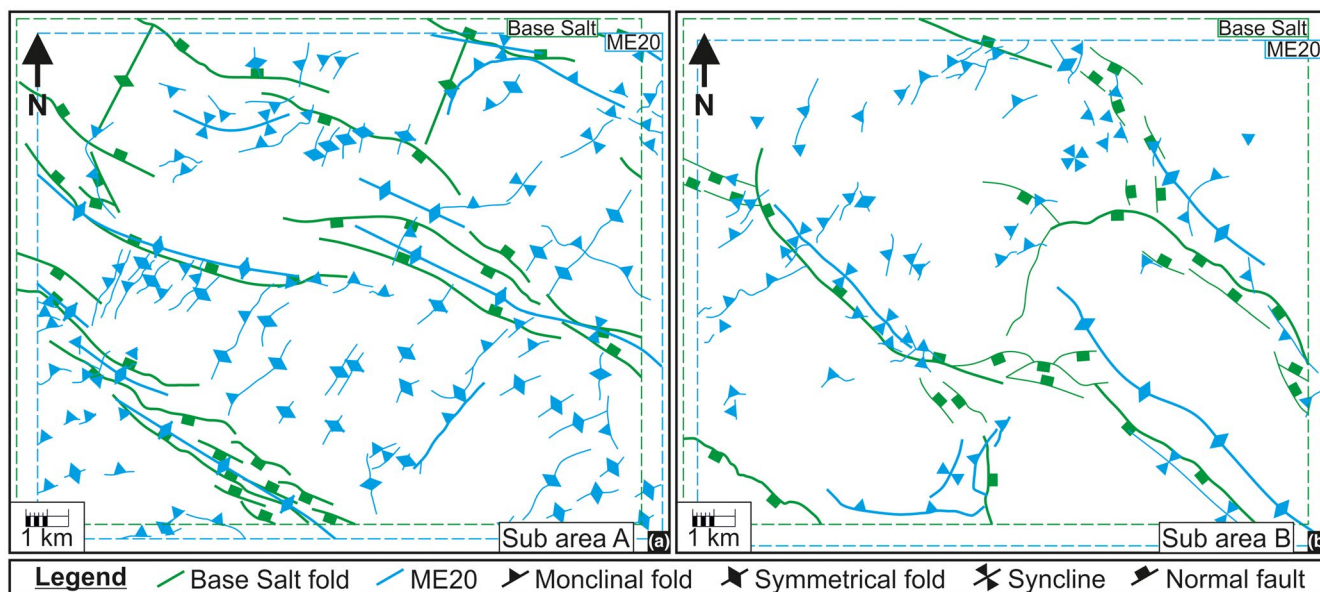


FIGURE 15 Map restoration of ME20 relative to the Base Salt in subareas A and B (see Figure 4 for subarea locations). (a and b) The map restorations show a strong alignment of normal faults at the Base Salt and NW-SE oriented folds and synclines at ME20. Other NE-SW symmetrical and monoclinical folds appear unrelated to the Base Salt faults and are oriented perpendicular to the recent salt flow direction [Colour figure can be viewed at wileyonlinelibrary.com]

restored strain pattern for the Late Messinian phase (Phase 1) is thus radically different to the final strain following the addition of the simple shear overprint. This has significant implications for future studies that aim to investigate the regional drivers for syn-Messinian salt flow and the resulting deformational response.

5.2 | Are shortening estimates invalid?

The dominance of upright symmetrical folds and far fewer asymmetric to recumbent folds following retro-deformation, along with the preservation of structural intersections between fold axes raises some challenging questions regarding the drivers for the Phase 1 deformation that would be impossible to tackle without having first removed the late stage simple shear. The overprinting of the Phase 2 simple shear on a more upright folded evaporite stratigraphy clearly distorts the fold geometry and results in higher apparent values of shortening that at first sight gives the impression of an increased contractional strain experienced by the salt in the Phase 2. However, the low strains in the overburden of <1% shortening combined with the full coupling of Top Salt to the overburden (Cartwright et al., 2018) mean that only very minor shortening could have occurred in the later, translational phase possibly explaining some of the minor reverse shear zones. Hence, there is an apparent paradox of an increase of apparent contractional strain accruing within the salt during Phase 2. The true shortening strain embedded into

the final deformed intra-Messinian deformation therefore only accrued in Phase 1, prior to or during the formation of the IMTS (Kirkham et al., 2020).

The superimposition of a late simple shear on an already folded multilayer is well known to result in significant errors in shortening estimation, if the later shear is not recognised (Carey, 1962; Sanderson, 1979; Wynne-Edwards, 1963). Simple shear on a previously folded layer dramatically increases the apparent shortening of that layer, but this is because line length is not conserved during the simple shear. As is well known from studies of the deformation of ice sheets (Hudleston, 2015), the distortion of passive objects within the flowing medium is a simple consequence of differential velocity vertically through the layer, even though the shear strain itself may be constant. If a layer is mechanically passive (see Fossen, 2016, p. 227), then line length is certainly not conserved during the simple shear deformation. Originally upright folds will deform into highly recumbent forms, with rotation of axial planes matching the shear angle (see Alsop et al., 2020). These shear folds are a specific category of flow folds in which the flow is at an angle to the axial plane as opposed to parallel to the axial plane (Hudleston, 2015). Previous studies in which line length balancing has been used to quantify the vertical strain distribution within the deformed Messinian Evaporites (Allen et al., 2016; Cartwright et al., 2012; Feng et al., 2017) are thus strictly invalid simply because a simple shear does not by itself result in any shortening parallel to the translation direction.

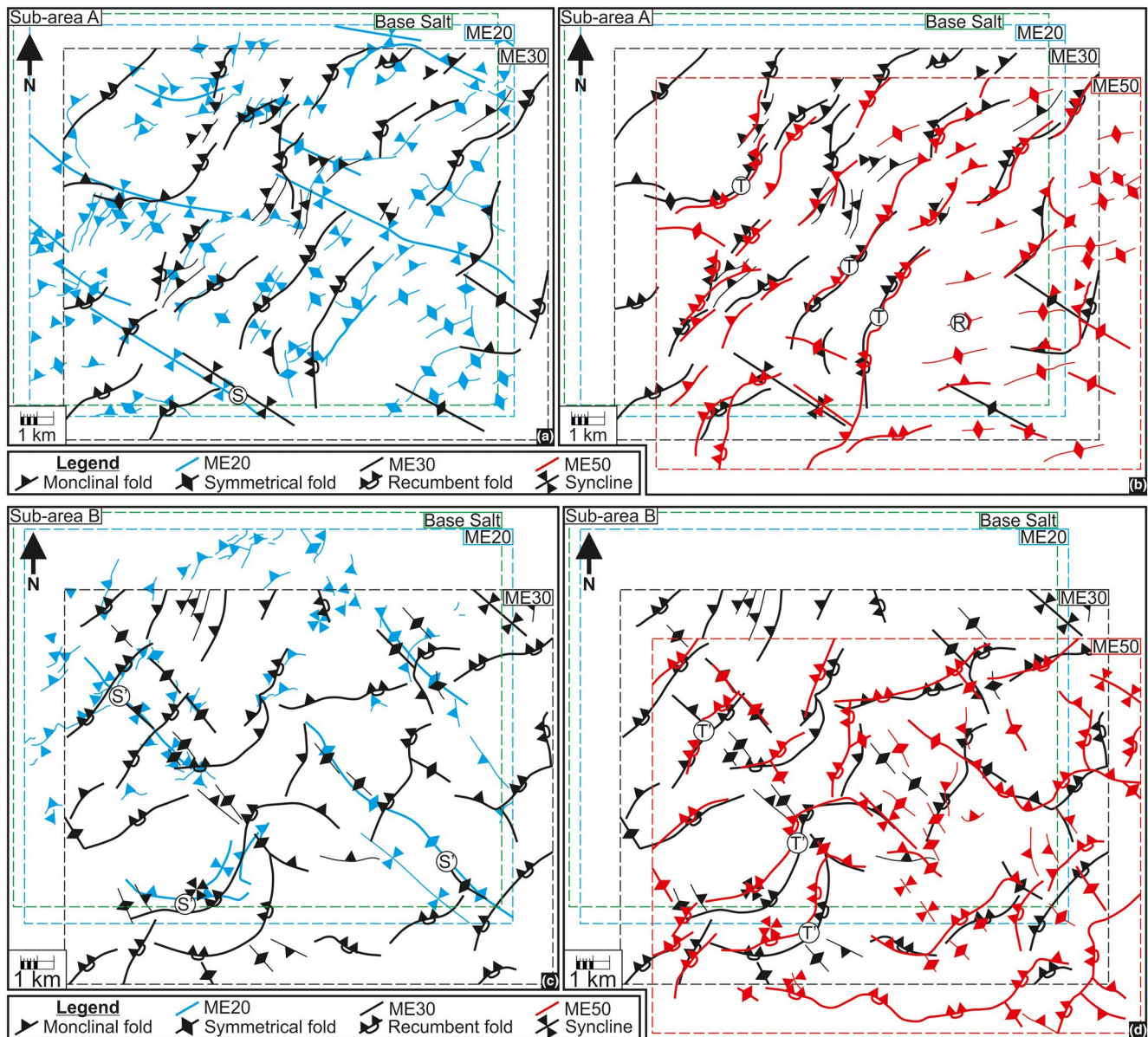


FIGURE 16 Map restorations in subareas A and B (see Figure 4 for location). (a) Map restoration of ME20 and ME30 in subarea A (the Base Salt structure map position is also shown). Some of the folds show some near vertical alignment (see label S); however, most do not, implying a detachment between the two horizons (within ME-II). (b) Map restoration of ME30 and ME50 in subarea A (the position of the Base Salt map and restored position of the ME20 map are also shown) shows a vertical alignment between the principle fold axes (see labels T). Minor structures that do not align (see label R) appear to detach within ME-IV. (c) Map restoration of ME20 and ME30 in subarea B (the Base Salt structure map position is also shown). A greater number of major folds, compared to subarea A, show some alignment following restoration (see label S'); however, most do not. (d) Map restoration of ME30 and ME50 in subarea B (the position of the Base Salt map and restored position of the ME20 map are also shown) shows a vertical alignment between the principle fold axes and some structural intersections (see labels T'). Similar to in sub study A, some minor folds do not align [Colour figure can be viewed at wileyonlinelibrary.com]

5.3 | Implications for Late Messinian deformational regime

In our study area, there may well have been more than one driver contributing to the folding that occurred during Phase 1, since there is contemporaneous shortening in multiple orientations (e.g., Figure 16c,d). There is no evidence that the intra-salt reflections acted as mechanical struts,

but those reflective intervals may have had a different bulk viscosity than the non-reflective layers. The low effective stress in these thin layers might support a view of their role as passive layers (see Section 3) with low competency that exerted little direct mechanical influence on deformation of the salt sheet, but nevertheless influencing rheology sufficiently to lead to localisation of detachments. A comparison of restored and unrestored sections drawn parallel to

the NW directed Couette flow also show that structures that appeared to be completely detached in the unrestored state (Figures 11a and 12a) can more plausibly be connected in the restored section (Figures 11b and 12b), possibly obviating the need to invoke some of the intra-Messinian detachments that would have been interpreted based on the unrestored structure. However, the increase in deformation structures in the different reflective layers upward through the salt implies increasing strain and detachment of smaller deformation structures. It is conceivable that whether a structure detaches in the salt or not depends on the magnitude of the deformation, with many of the smaller structures with lower displacement (such as the reverse shear zones) failing to propagate through the thick, halite rich layers (Figures 8 and 16b).

One of the most striking features of the intra-Messinian deformation around the Levant Basin is the almost ubiquitous development of recumbent folds or low-angle shear zones. These low-angle shear zones have previously been interpreted as thrust faults (Cartwright et al., 2012; Feng et al., 2017; Gradmann et al., 2005), but it seems more likely that in the halite dominated succession present in the Levant Basin, they are ductile shear zones and not brittle faults per se (Jackson et al., 2015; Talbot, 1979). As we have shown with the restorations (Figures 11 and 12), the superimposition of shear strains of >0.8 means that recumbent folds are an inevitable consequence of the translational simple shear of early-formed upright folds. Since we can definitely calibrate the flow regime in the North Levant Basin using five separate fluid escape pipe trails, we can infer that all the NW verging recumbent folds (Figures 10, 13 and 14) in the area covered by this flow domain formed in this way. Extrapolating this methodology to the rest of the basin, we suggest that it is plausible that all the areas with a dominance of recumbent folding also experienced Couette flow during Phase 2 deformation. Thrust vergence and fold strike have both been used as kinematic indicators for flow direction in previous studies (Cartwright et al., 2012; Feng et al., 2017) but not specifically as kinematic indicators of flow regime. This suggestion needs further testing and independent calibration, but if valid, it could be used in any salt basin where internal deformation of salt is visible on seismic data.

5.4 | The use of map restoration as a tool to constrain flow regime in salt

The fluid escape pipe trails identified in the North Levant Basin have provided invaluable constraints on the local kinematics of a salt sheet deforming under a regional tilt (Kirkham et al., 2019). However, they only provide direct kinematic constraints in the immediate surrounds of the

trails. In a salt basin where flow patterns and regimes may vary quite significantly over short lateral distances, it would be invaluable to use another tool to constrain the kinematics. Here, we have shown that map restoration (Figures 15 and 16) from different levels also provides additional confirmation that the Couette flow occurs within a broad region with a uniform flow direction rather than just within a narrow corridor as defined by the fluid escape pipe trails.

A further biproduct of map restoration of intra-salt markers is that by restoring maps to their correct positions, it is then possible to identify mapped relationships from horizon to horizon that were not visible in the final deformed, and unrestored state (Figure 16). This means that sedimentary or structural features that may have been seemingly unconnected are now more plausibly connected in the restored configuration. Offset structures within a salt layer (particularly those with distinct geometries or intersect) can therefore be used as kinematic markers to assist in interpretation of the salt flow profile. Where structures cannot be matched after restoration, a case can be made more strongly that some internal detachments must have been functioning to partition the strain during the original deformation or that there are significant rheological changes through the salt sheet.

5.5 | Wider application to other salt basins

One of the most fundamental implications of this study, with wide potential application is the realisation that extremely high strains can be concealed from view by the lens of the seismic method if they are shear strains. Without the benefit of the fluid escape pipe trails overlying the Oceanus and Saida-Tyr pre-salt folds to reveal the scale of the shear strain, it is unlikely that the recumbent folding would be seen as a consequence of a superimposed simple shear, and as in older studies been simply taken as evidence for a single phase of deformation occurring entirely within the Messinian. Obscuring of the true strain in salt tectonic deformation must be present in many other salt basins, perhaps concealed even further from interpretation by even later phases of deformation. Couette or Poiseuille flow involves shearing within and parallel to the salt layer boundaries, so we can expect similar distortional geometries to occur wherever lateral flow of salt occurs.

6 | CONCLUSIONS

In this study, we have used cross sections and mapped surfaces from 3D seismic reflection data to present a detailed description and analysis of intra-salt structures within the Messinian Evaporites in the North Levant Basin, Eastern Mediterranean. The Messinian Evaporites have been deformed during two main deformational phases, one during

Late Messinian, and a later phase during the Late Pliocene to Recent. This most recent phase of deformation has been calibrated by five fluid escape pipe trails in the North Levant Basin that emanate from pre-salt anticlines, transect the thick Messinian Evaporites and have pockmarks at their outlets that formed at contemporaneous seafloors during the Late Pliocene to Recent. The once vertical fluid escape pipes within the translational domain of the salt basin have been deformed into a Couette (simple shear) geometry in the Messinian Evaporites by the flowing salt, and the pockmarks have been translated NW in the basinward salt flow direction. Using the simple shear implied for the Late Pliocene to Recent phase of deformation by the fluid escape pipe trails, we undertook cross section and map restorations to remove the overprint from this latest phase of deformation. Removal of the Late Pliocene to Recent phase of deformation retro-deformed intrasalt structures to their initial configuration following the Late Messinian phase of deformation. The major findings are as follows:

1. Retro-deformation cannot remove all the strain within the salt but results in far simpler predominantly upright folds, arguing against a single phase of deformation but in favour of the prior proposed two phase deformational model.
2. Structures that appeared to be completely detached in the unrestored state are shown to be connected in restored sections, in many instances obviating the need for detachments. Structures that are offset within a salt layer, particularly those with distinct geometries, but that reconnect following retro-deformation can be used as kinematic markers to assist in interpreting the salt flow profile.
3. Failure to recognise the late simple shear deformation of the salt layer results in a completely erroneous view of the deformational system. Retro-deformed intrasalt folds display contemporaneous shortening in multiple orientations following retro-deformation, with significant implication going forward for how intra-Messinian deformation and its drivers are interpreted.
4. Line length is not conserved during simple shear of passive layers and simple shear does not by itself result in any shortening parallel to the translation direction, rendering line length balancing invalid.
5. The true strain within a salt sheet can be obscured from view by the lens of the seismic method if augmented by shear strain. Obscuring of the true strain within a salt sheet must be present in many other salt basins and is perhaps shrouded further with even more deformation phases.

ACKNOWLEDGEMENTS

We are grateful to the editor Craig Magee and the reviewers Lidia Lonergan, Zohar Gvirtzman and an anonymous

reviewer for their insightful and very constructive comments that have led to improvements in the manuscript. We are grateful to TGS for provision of the 3D seismic data. We thank Schlumberger for provision of the seismic interpretation software.

CONFLICT OF INTEREST

There are no conflicts of interest to declare.

PEER REVIEW

The peer review history for this article is available at <https://publons.com/publon/10.1111/bre.12564>.

DATA AVAILABILITY STATEMENT

The data used for this research are confidential industry seismic reflection data and cannot be shared.

REFERENCES

- Albertz, M., & Ings, S. J. (2012). Some consequences of mechanical stratification in basin-scale numerical models of passive-margin salt tectonics. *Geological Society, London, Special Publications*, 363, 303–330. <https://doi.org/10.1144/SP363.14>
- Allen, H., Jackson, C.-A.-L., & Fraser, A. J. (2016). Gravity-driven deformation of a youthful saline giant: The interplay between gliding and spreading in the Messinian basins of the Eastern Mediterranean. *Petroleum Geoscience*, 22, 340–356. <https://doi.org/10.1144/petgeo2016-034>
- Alsop, G., Weinberger, R., Marco, S., & Levi, T. (2020). Folding during soft-sediment deformation. *Geological Society, London, Special Publications*, 487, 81–104. <https://doi.org/10.1144/SP487.1>
- Bar, O., Zilberman, E., Feinstein, S., Calvo, R., & Gvirtzman, Z. (2016). The uplift history of the Arabian Plateau as inferred from geomorphologic analysis of its northwestern edge. *Tectonophysics*, 671, 9–23.
- Ben Zeev, Y., & Gvirtzman, Z. (2020). When Two Salt Tectonics Systems Meet: Gliding downslope the levant margin and salt out-squeezing from under the Nile delta. *Tectonics*, 39, e2019TC005715.
- Ben-Avraham, Z. (1978). The structure and tectonic setting of the Levant continental margin, Eastern Mediterranean. *Tectonophysics*, 46, 313–331. [https://doi.org/10.1016/0040-1951\(78\)90210-X](https://doi.org/10.1016/0040-1951(78)90210-X)
- Berkhout, A. J. (1984). *Seismic resolution: A quantitative analysis of resolving power of acoustical echo techniques*. Geophysical Press.
- Bertoni, C., & Cartwright, J. A. (2006). Controls on the basinwide architecture of late Miocene (Messinian) evaporites on the Levant margin (Eastern Mediterranean). *Sedimentary Geology*, 188, 93–114. <https://doi.org/10.1016/j.sedgeo.2006.03.019>
- Bertoni, C., & Cartwright, J. (2007). Major erosion at the end of the Messinian Salinity Crisis: Evidence from the Levant Basin, Eastern Mediterranean. *Basin Research*, 19, 1–18. <https://doi.org/10.1111/j.1365-2117.2006.00309.x>
- Brown, A. R. (2011). *Interpretation of three-dimensional seismic data*. Society of Exploration Geophysicists and American Association of Petroleum Geologists.
- Brun, J.-P., & Fort, X. (2011). Salt tectonics at passive margins: Geology versus models. *Marine and Petroleum Geology*, 28, 1123–1145. <https://doi.org/10.1016/j.marpetgeo.2011.03.004>

- Brun, J. P., & Merle, O. (1985). Strain patterns in models of spreading-gliding Nappes. *Tectonics*, 4, 705–719. <https://doi.org/10.1029/TC004i007p00705>
- Carey, S. W. (1962). Folding. *Bulletin of Canadian Petroleum Geology*, 10, 95–144.
- Cartwright, J. A., & Jackson, M. (2008). Initiation of gravitational collapse of an evaporite basin margin: The Messinian saline giant, Levant Basin, eastern Mediterranean. *Geological Society of America Bulletin*, 120, 399–413. <https://doi.org/10.1130/B26081X.1>
- Cartwright, J., Jackson, M., Dooley, T., & Higgins, S. (2012). Strain partitioning in gravity-driven shortening of a thick, multilayered evaporite sequence. *Geological Society, London, Special Publications*, 363, 449–470. <https://doi.org/10.1144/SP363.21>
- Cartwright, J., Kirkham, C., Bertoni, C., Hodgson, N., & Rodriguez, K. (2018). Direct calibration of salt sheet kinematics during gravity-driven deformation. *Geology*, 46, 623–626. <https://doi.org/10.1130/G40219.1>
- Elfassi, Y., Gvirtzman, Z., Katz, O., & Aharonov, E. (2019). Chronology of post-Messinian faulting along the Levant continental margin and its implications for salt tectonics. *Marine and Petroleum Geology*, 109, 574–588. <https://doi.org/10.1016/j.marpetgeo.2019.05.032>
- Feng, Y. E., Steinberg, J., & Reshef, M. (2017). Intra-salt deformation: Implications for the evolution of the Messinian evaporites in the Levant Basin, eastern Mediterranean. *Marine and Petroleum Geology*, 88, 251–267. <https://doi.org/10.1016/j.marpetgeo.2017.08.027>
- Feng, Y. E., Yankelzon, A., Steinberg, J., & Reshef, M. (2016). Lithology and characteristics of the Messinian evaporite sequence of the deep Levant Basin, eastern Mediterranean. *Marine Geology*, 376, 118–131. <https://doi.org/10.1016/j.marpetgeo.2016.04.004>
- Fiduk, J. C., & Rowan, M. G. (2012). Analysis of folding and deformation within layered evaporites in Blocks BM-S-8 & -9, Santos Basin, Brazil. *Geological Society, London, Special Publications*, 363, 471–487. <https://doi.org/10.1144/SP363.22>
- Fossen, H. (2016). *Structural geology*. Cambridge University Press.
- Garcia-Castellanos, D., Estrada, F., Jiménez-Munt, I., Gorini, C., Fernández, M., Vergés, J., & de Vicente, R. (2009). Catastrophic flood of the Mediterranean after the Messinian salinity crisis. *Nature*, 462, 778–781. <https://doi.org/10.1038/nature08555>
- Gardosh, M. A., & Druckman, Y. (2006). Seismic stratigraphy, structure and tectonic evolution of the Levantine Basin, offshore Israel. *Geological Society, London, Special Publications*, 260, 201–227. <https://doi.org/10.1144/GSL.SP.2006.260.01.09>
- Gemmer, L., Ings, S. J., Medvedev, S., & Beaumont, C. (2004). Salt tectonics driven by differential sediment loading: Stability analysis and finite-element experiments. *Basin Research*, 16, 199–218. <https://doi.org/10.1111/j.1365-2117.2004.00229.x>
- Ghalayini, R., Homberg, C., Daniel, J., & Nader, F. (2017). Growth of layer-bound normal faults under a regional anisotropic stress field. *Geological Society, London, Special Publications*, 439, 57–78. <https://doi.org/10.1144/SP439.13>
- Ghalayini, R., Nader, F. H., Bou Daher, S., Hawie, N., & Chbat, W. E. (2018). Petroleum systems of Lebanon: An update and review. *Journal of Petroleum Geology*, 41, 189–214. <https://doi.org/10.1111/jpg.12700>
- Gradmann, S., Hübscher, C., Ben-Avraham, Z., Gajewski, D., & Netzeband, G. (2005). Salt tectonics off northern Israel. *Marine and Petroleum Geology*, 22, 597–611. <https://doi.org/10.1016/j.marpetgeo.2005.02.001>
- Gvirtzman, Z., Manzi, V., Calvo, R., Gavrieli, I., Gennari, R., Lugli, S., Reghizzi, M., & Roveri, M. (2017). Intra-Messinian truncation surface in the Levant Basin explained by subaqueous dissolution. *Geology*, 45, 915–918. <https://doi.org/10.1130/G39113.1>
- Gvirtzman, Z., Reshef, M., Buch-Leviatan, O., & Ben-Avraham, Z. (2013). Intense salt deformation in the Levant Basin in the middle of the Messinian Salinity Crisis. *Earth and Planetary Science Letters*, 379, 108–119. <https://doi.org/10.1016/j.epsl.2013.07.018>
- Hall, J., Calon, T., Aksu, A., & Meade, S. (2005). Structural evolution of the Latakia Ridge and Cyprus Basin at the front of the Cyprus Arc, eastern Mediterranean Sea. *Marine Geology*, 221, 261–297. <https://doi.org/10.1016/j.marpetgeo.2005.03.007>
- Hübscher, C., Cartwright, J., Cypionka, H., Delange, G. J., Robertson, A., Suc, J. P., & Urai, J. L. (2007). Global look at salt giants. *Eos, Transactions American Geophysical Union*, 88, 177–179. <https://doi.org/10.1029/2007EO160002>
- Hudleston, P. J. (2015). Structures and fabrics in glacial ice: A review. *Journal of Structural Geology*, 81, 1–27. <https://doi.org/10.1016/j.jsg.2015.09.003>
- Jackson, C.-A.-L., Jackson, M. P., Hudec, M. R., & Rodriguez, C. R. (2015). Enigmatic structures within salt walls of the Santos Basin—Part 1: Geometry and kinematics from 3D seismic reflection and well data. *Journal of Structural Geology*, 75, 135–162. <https://doi.org/10.1016/j.jsg.2015.01.010>
- Kartveit, K. H., Omosanya, K. O., Johansen, S. E., Eruteya, O., Reshef, M., & Waldmann, N. D. (2018). Multiphase structural evolution and geodynamic implications of Messinian salt-related structures, Levant Basin, Offshore Israel. *Tectonics*, 37(5), 1210–1230. <https://doi.org/10.1029/2017TC004794>
- Kirkham, C., Bertoni, C., Cartwright, J., Lensky, N. G., Sirota, I., Rodriguez, K., & Hodgson, N. (2020). The demise of a ‘salt giant’ driven by uplift and thermal dissolution. *Earth and Planetary Science Letters*, 531, <https://doi.org/10.1016/j.epsl.2019.115933>
- Kirkham, C., Cartwright, J., Bertoni, C., Rodriguez, K., & Hodgson, N. (2019). 3D kinematics of a thick salt layer during gravity-driven deformation. *Marine and Petroleum Geology*, 110, 434–449. <https://doi.org/10.1016/j.marpetgeo.2019.07.036>
- Kirkham, C., Cartwright, J., Hermanrud, C., & Jebsen, C. (2018). The genesis of mud volcano conduits through thick evaporite sequences. *Basin Research*, 30, 217–236. <https://doi.org/10.1111/bre.12250>
- Krijgsman, W., Hilgen, F., Raffi, I., Sierro, F. J., & Wilson, D. (1999). Chronology, causes and progression of the Messinian salinity crisis. *Nature*, 400, 652. <https://doi.org/10.1038/23231>
- Lofi, J. (2018). *Seismic Atlas of the Messinian Salinity Crisis markers in the Mediterranean Sea* (Vol. 2). Société Géologique de France.
- Lofi, J., Sage, F., Déverchère, J., Loncke, L., Maillard, A., Gaullier, V., Thinon, I., Gillet, H., Guennoc, P., & Gorini, C. (2011). Refining our knowledge of the Messinian salinity crisis records in the offshore domain through multi-site seismic analysis. *Bulletin De La Société Géologique De France*, 182, 163–180. <https://doi.org/10.2113/gssgfbull.182.2.163>
- Løseth, H., Wensaas, L., Arntsen, B., Hanken, N.-M., Basire, C., & Graue, K. (2011). 1000 m long gas blow-out pipes. *Marine and Petroleum Geology*, 28, 1047–1060.
- Madof, A. S., Bertoni, C., & Lofi, J. (2019). Discovery of vast fluvial deposits provides evidence for drawdown during the late Miocene Messinian salinity crisis. *Geology*, 47, 171–174. <https://doi.org/10.1130/G45873.1>
- Maillard, A., Hübscher, C., Benkhelil, J., & Tahchi, E. (2011). Deformed Messinian markers in the Cyprus Arc: Tectonic and/or Messinian Salinity Crisis indicators? *Basin Research*, 23, 146–170. <https://doi.org/10.1111/j.1365-2117.2010.00464.x>
- Manzi, V., Gennari, R., Hilgen, F., Krijgsman, W., Lugli, S., Roveri, M., & Sierro, F. J. (2013). Age refinement of the Messinian salinity

- crisis onset in the Mediterranean. *Terra Nova*, 25, 315–322. <https://doi.org/10.1111/ter.12038>
- Meilijson, A., Hilgen, F., Sepúlveda, J., Steinberg, J., Fairbank, V., Flecker, R., Waldmann, N. D., Spaulding, S. A., Bialik, O. M., Boudinot, F. G., Illner, P., & Makovsky, Y. (2019). Chronology with a pinch of salt: Integrated stratigraphy of Messinian evaporites in the deep Eastern Mediterranean reveals long-lasting halite deposition during Atlantic connectivity. *Earth-Science Reviews*, 194, 374–398. <https://doi.org/10.1016/j.earscirev.2019.05.011>
- Nader, F. H. (2011). The petroleum prospectivity of Lebanon: An overview. *Journal of Petroleum Geology*, 34, 135–156. <https://doi.org/10.1111/j.1747-5457.2011.00498.x>
- Netzeband, G., Hübscher, C., & Gajewski, D. (2006). The structural evolution of the Messinian evaporites in the Levantine Basin. *Marine Geology*, 230, 249–273. <https://doi.org/10.1016/j.margeo.2006.05.004>
- Oppo, D., Evans, S., Iacopini, D., Kabir, S. M., Maselli, V., & Jackson, C.-A.-L. (2020). Leaky salt: Pipe trails record the history of cross-evaporite fluid escape in the northern Levant Basin, Eastern Mediterranean. *Basin Research*. <https://doi.org/10.1111/bre.12536>
- Osborne, M. J., & Swarbrick, R. E. (1997). Mechanisms for generating overpressure in sedimentary basins: A reevaluation. *AAPG Bulletin*, 81, 1023–1041. <https://doi.org/10.1306/522B49C9-1727-11D7-8645000102C1865D>
- Peel, F. J. (2014). The engines of gravity-driven movement on passive margins: Quantifying the relative contribution of spreading vs. gravity sliding mechanisms. *Tectonophysics*, 633, 126–142. <https://doi.org/10.1016/j.tecto.2014.06.023>
- Reiche, S., Hübscher, C., & Beitz, M. (2014). Fault-controlled evaporite deformation in the Levant Basin, Eastern Mediterranean. *Marine Geology*, 354, 53–68. <https://doi.org/10.1016/j.margeo.2014.05.002>
- Rowan, M. G., Peel, F. J., & Vendeville, B. C. (2004). Gravity-driven fold belts on passive margins. In K. R. McClay (Ed.), *Thrust and hydrocarbon systems: AAPG Memoir* (Vol. 82, pp. 157–182). American Association of Petroleum Geologists.
- Rowan, M. G., Urai, J. L., Fiduk, J. C., & Kukla, P. A. (2019). Deformation of intrasalt competent layers in different modes of salt tectonics. *Solid Earth*, 10(987–1013), 2019. <https://doi.org/10.5194/se-10-987-2019>
- Ryan, W. B., & Cita, M. B. (1978). The nature and distribution of Messinian erosional surfaces—Indicators of a several-kilometer-deep Mediterranean in the Miocene. *Marine Geology*, 27, 193–230. [https://doi.org/10.1016/0025-3227\(78\)90032-4](https://doi.org/10.1016/0025-3227(78)90032-4)
- Ryan, W., Cita, M., & Hsü, H. (1973). The origin of the Mediterranean evaporates. *Initial Reports of the Deep Sea Drilling Project*, 13, 1203–1231.
- Sanderson, D. J. (1979). The transition from upright to recumbent folding in the Variscan fold belt of southwest England: A model based on the kinematics of simple shear. *Journal of Structural Geology*, 1, 171–180. [https://doi.org/10.1016/0191-8141\(79\)90037-3](https://doi.org/10.1016/0191-8141(79)90037-3)
- Talbot, C. J. (1979). Fold trains in a glacier of salt in southern Iran. *Journal of Structural Geology*, 1, 5–18. [https://doi.org/10.1016/0191-8141\(79\)90017-8](https://doi.org/10.1016/0191-8141(79)90017-8)
- Van Gent, H., Urai, J. L., & de Keijzer, M. (2011). The internal geometry of salt structures—a first look using 3D seismic data from the Zechstein of the Netherlands. *Journal of Structural Geology*, 33, 292–311. <https://doi.org/10.1016/j.jsg.2010.07.005>
- Wynne-Edwards, H. (1963). Flow folding. *American Journal of Science*, 261, 793–814.
- Zucker, E., Gvirtzman, Z., Steinberg, J., & Enzel, Y. (2020). Salt tectonics in the Eastern Mediterranean Sea: Where a giant delta meets a salt giant. *Geology*, 48, 134–138. <https://doi.org/10.1130/G47031.1>

SUPPORTING INFORMATION

Additional Supporting Information may be found online in the Supporting Information section.

How to cite this article: Kirkham C, Cartwright J. Restoration of multiphase salt tectonic deformation using passive strain markers. *Basin Res.* 2021;33: 2453–2473. <https://doi.org/10.1111/bre.12564>